International Journal of Pharmaceutics 649 (2024) 123663

Contents lists available at ScienceDirect

International Journal of Pharmaceutics

journal homepage: www.elsevier.com/locate/ijpharm

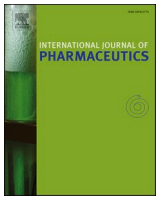

Targeted DPPC/DMPG surface-modified voriconazole lipid nanoparticles control invasive pulmonary aspergillosis in immunocompromised population: *in-vitro* and *in-vivo* assessment

Heba A. Fayyaz [a], Magda A. EL-Massik [a], Mohammed Bahey-El-Din [b], Amany Abdel-Bary [c], Ossama Y. Abdallah [a], Hoda M. Eltaher [a,d,*]

[a] Department of Pharmaceutics, Faculty of Pharmacy, Alexandria University, 21521, Egypt
[b] Department of Microbiology and Immunology, Faculty of Pharmacy, Alexandria University, Alexandria 21521, Egypt
[c] Department of Pathology, Faculty of Medicine, Alexandria University, Alexandria 21131, Egypt
[d] Regenerative Medicine and Cellular Therapies Division, School of Pharmacy, Faculty of Science, University of Nottingham, Nottingham NG7 2RD, United Kingdom

ARTICLE INFO

Keywords:
Dipalmitoylphosphatidylcholine
Dimyristoylphosphatidylglycerol
Prophylaxis
Voriconazole
Invasive Pulmonary Aspergillosis
Immunocompromised
Targeted Delivery

ABSTRACT

Invasive pulmonary aspergillosis (IPA) is the most devastating Aspergillus-related lung disease. Voriconazole (VRZ) is the first-line treatment against IPA. Despite availability in oral and parenteral dosage forms, risks of systemic toxicity dictate alternative pulmonary administration. Inspired by natural lung surfactants, dipalmitoylphosphatidylcholine/dimyristoylphosphatidylglycerol (DPPC/DMPG) surface-modified lipid nanoparticles (LNPs) were scrutinized for pulmonary administration. DPPC/DMPG-VRZ-LNPs prepared using ultrasonication/thin film hydration were investigated for colloidal properties over 3-month shelf storage. They were stable with a slight change in entrapment efficiency. They provided a sustained VRZ release over 24 h, with a rapid initial release. *In vitro* aerosolization indicated higher percentages of VRZ deposited on stages corresponding to secondary bronchi and alveolar ducts. Moreover, intrapulmonary administration maintained high lung VRZ concentration (27 ± 1.14 μg/g) after 6 h. A preclinical study using a cyclophosphamide-induced neutropenic rat model demonstrated a 3-fold reduction in BALF-Galactomannan down to 0.515 ± 0.22 μg/L confirming DPPC/DMPG-VRZ-LNPs potential in hyphal growth inhibition. Histopathological examination of infected/nontreated lung sections exhibited dense fungal load inside alveoli and blood vessels indicating massive tissue and angioinvasiveness. Nevertheless, DPPC/DMPG-VRZ-LNPs-treated animals displayed minimal hyphae with no signs of invasiveness. The developed bioinspired nanoparticles serve as prospective bioactive nanocarrier candidates for pulmonary administration of VRZ in the management of IPA.

1. Introduction

Aspergillosis refers to a variety of conditions caused by saprotrophic filamentous fungi that are found in air, soil and growing on decaying organic debris (Mousavi et al., 2016). The most common etiological species are ***A. fumigatus*** followed by ***A. flavus***, ***A. niger***, and ***A. terreus*** (Zakaria et al., 2020). Inhalation of the airborne spores is the primary route of *Aspergillus* infections where produced conidia are small enough to reach deep into human airways and pulmonary alveoli. In a healthy host, fungal spores are rapidly cleared from the respiratory tract. However, in patients with an immune defect, the spores persist, colonize, and eventually lead to the development of pulmonary aspergillosis clinical conditions.

Pulmonary Aspergillosis **(PA)** is a broad term that encompasses a wide spectrum of clinical syndromes ranging from non-invasive aspergilloma and allergic bronchopulmonary aspergillosis (**ABPA)** to semi-invasive and invasive infections such as chronic necrotizing aspergillosis (**CNA**) and invasive pulmonary aspergillosis (**IPA**) respectively (Chabi et al., 2015; Kousha et al., 2011). The major predisposing factors are the host's lung allergic status e.g. asthma, airway diseases; bronchial

* Corresponding author.
E-mail addresses: Heba.fayyaz@alexu.edu.eg (H.A. Fayyaz), magda.elmassik@alexu.edu.eg (M.A. EL-Massik), m.bahey-el-din@alexu.edu.eg (M. Bahey-El-Din), Amany.abdelbary@alex.edu.eg (A. Abdel-Bary), ossama.youssef@alexu.edu.eg (O.Y. Abdallah), hoda.eltaher@nottingham.ac.uk, hoda.amin@alexpharmacy.edu.eg (H.M. Eltaher).

https://doi.org/10.1016/j.ijpharm.2023.123663
Received 20 July 2023; Received in revised form 21 November 2023; Accepted 30 November 2023
Available online 5 December 2023

dilatation and cystic fibrosis, chronic lung cavities like tuberculosis or sarcoidosis, and immune deficiency (Chabi et al., 2015). Among these syndromes, IPA is considered as the most devastating *Aspergillus*-related lung disease with a rapidly evolving epidemiology (Latgé and Chamilos, 2019; Verweij et al., 2020). The global incidence of IPA was reported to be higher than 300,000 cases per year with an associated mortality rate ranging from 40 to 90 % with a high economic burden (Firacative, 2020). High-risk groups are individuals with hematological malignancies (Ma et al., 2022), COPD, patients on long-term corticosteroid therapy, individuals with inherited immunodeficiencies, and individuals infected with human immunodeficiency virus (Budin et al., 2021).

According to the Society of Infectious Diseases guidelines, voriconazole (**VRZ**) is recommended as the first-line treatment for the therapeutic and prophylactic management of IPA (Kaur et al., 2021). For instance, the 90-day mortality rates of IPA patients with hematologic conditions were 46 and 59.3 % when voriconazole was administered for prophylaxis or not, respectively (Budin et al., 2021). VRZ is a second-generation triazole derivative that is currently available in conventional dosage forms for oral and parenteral administration only. The recommended clinical dose for the management of IPA is 6 mg/kg IV twice daily for the first 24 h, followed by 4 mg/kg IV or 200 mg PO twice daily. Higher paediatric dosing (7 mg/kg twice daily intravenously or 200 mg PO twice daily, both without loading doses) reflects the rapid metabolism and linear kinetics in the paediatric population (Lat and Thompson, 2011). However, VRZ kinetics in children remain controversial (Chen et al., 2022; Michael et al., 2010; Walsh et al., 2004). VRZ demonstrates a potent extended spectrum of activity against many opportunistic and resistant fungal pathogens (Jović et al., 2019). VRZ's broader spectrum of activity is often compromised with increased pharmacokinetic variability, risk of drug interactions, unique adverse effects, and systemic toxicity (Bellmann and Smuszkiewicz, 2017; Orssaud et al., 2021).

Pulmonary delivery represents an appealing route of drug administration for direct delivery to the lung, overcoming systemic toxicities, achieving higher drug levels with much lower doses, and reducing side effects and drug-drug interactions (Borghardt et al., 2018). Eventually, this maximizes the treatment impact and reduces the risk of developing resistance. Nevertheless, the airway geometry and defense mechanisms pose a challenge for successful pulmonary delivery (Mishra and Singh, 2020). Nanoparticle-based drug delivery systems are developed to circumvent such shortcomings by bypassing extrapulmonary and intracellular pulmonary barriers, protecting the encapsulated drugs, and achieving targeting with increased bioavailability (Pramanik et al., 2021).

Lipid nanoparticles (**LNPs**) provide a highly versatile platform that can support and overcome the limitation of a wide range of drugs such as solubility, permeability, stability, and cellular interactions. Such versatility emerges from the variety of excipients recruited in their formulation including lipids with different charges, rigidities and activities, surfactants, and co-surfactants among others (Nakmode et al., 2022). LNPs exhibit many advantages over polymeric nanoparticles including better biocompatibility, affordability, scaling-up capabilities, and tolerability in the airways since lipids are considered the major component of the lung surfactant (Fisher, 2015; Ghasemiyeh and Mohammadi-Samani, 2018). Pulmonary surfactant is a lipoprotein complex, with 90 % of its mass being lipid. Phospholipids (**PL**), especially phosphatidylcholine (**PC**) and more specifically dipalmitoylphosphatidylcholine (**DPPC**), are the main lipid species responsible for the surface tension-reduction properties (Agudelo et al., 2020).

DPPC is recognized as a **GRAS** excipient for pulmonary delivery by the FDA (Wauthoz and Amighi, 2014). It plays a vital role in maintaining the conducting airways patency in the lungs, preventing cohesiveness of bronchiolar walls via preserving the watery lining outspreading and reducing the mucus film surface tension (Chen et al., 2019; Joshi et al., 2014). DPPC-containing formulations benefit from the spreading behavior of surfactants to achieve uniform drug reach to the remote alveolar areas, minimizing premature mucociliary clearance and improving internalization at the air-lung interface. In this context, they display improved retention, alleviate compromised lung compliance, and maintain alveolar stability (El-Sherbiny et al., 2011; Hidalgo et al., 2020; Kaur et al., 2021; Muralidharan et al., 2015). Additionally, DPPC prevents system opsonization by camouflaging the macrophages (Guagliardo et al., 2018; Osman et al., 2013). Moreover, the aerosol performance of inhalable spray-dried particles can be boosted by the incorporation of minimal amounts of DPPC resulting in effective inhalation therapy (Cuvelier et al., 2015; Duan et al., 2013).

Integration of the pulmonary-active DPPC into VRZ-loaded nanoparticles comes as a biomimetic approach to increase particles' tolerability for pulmonary delivery and to minimize the risk of macrophage uptake, thereby facilitating nanoparticles' diffusion and internalization. DPPC-surface active polymer hybrid nanoparticles for pulmonary delivery of voriconazole have been recently reported to augment VRZ pulmonary deposition and retention (Kaur et al., 2021). Herein, we develop novel DPPC/DMPG surface-modified lipid nanoparticles to achieve high local and controlled pulmonary VRZ concentrations using low VRZ doses (1 mg/kg) to maximize the treatment impact and limit the extent of disease invasiveness. The inclusion of a key formulation modifier (DMPG) as an adsorption enhancer maintains the stability, mono-dispersibility, and spray drying/aerosolization outcomes. A comprehensive toolset of *in vitro* studies has been recruited to assess the feasibility of DPPC/DMPG surface-modified lipid nanoparticles for pulmonary delivery of VRZ in terms of colloidal properties, solid-state characteristics, drug content and release, storage-stability, antifungal activity, spray drying and *in vitro* lung deposition. These have been complemented with an *in vivo* lung retention study and a detailed, comprehensive disease-state animal study to assess the nanocarrier system *in vivo* antifungal therapeutic potential in an immunocompromised population.

2. Materials and methods

2.1. Materials

Voriconazole (**VRZ**) was kindly gifted from Glenmark Pharmaceuticals Ltd., Mumbai, India. Compritol 888 ATO (**Compritol®**) was received as a gift from Gattefosse, Nanterre, France. Phospholipids including Dipalmitoylphosphatidylcholine **(DPPC)** and dimyristoylphosphatidylglycerol **(DMPG)**, were kindly provided from Lipoid, Germany as a gift to support the project. Poloxamer 407 **(PLX 407)** and Poloxamer 188 **(PLX 188)** were purchased from BASF, Germany. Tween 80 was purchased from Sigma-Aldrich, Merck KGaA, Germany. Polyvinyl alcohol **(PVA)** with 1700 degrees of polymerization was obtained from Hayashi Pure Chemical Industries, Osaka, Japan. Sebouraud's Dextrose medium was supplied from HIMEDIA, India. Vivaspin 6 concentrators, 100 K MWCO, were purchased from Sartorius, Biotech Ltd., Göttingen, Germany. Visking Dialysis tubing of regenerated cellulose, MWCO 12–14 KDa, was purchased from SERVA, Germany. Acetonitrile (HPLC grade) was purchased from Fisher Scientific Inc., Hampton, USA. Formalin, analytical-grade organic solvents, and buffer salts were purchased from El-Nasr Pharmaceuticals, Egypt.

2.2. Preparation of voriconazole lipid nanoparticles

Plain and VRZ-loaded nanoparticles (VRZ-LNPs) were prepared by an ultrasonication technique (Vijayanand et al. (2018)). The lipid phase (Compritol®, 3 % w/v) was set to melt in a thermostatically controlled water bath adjusted to a temperature 5 °C above the melting point. A surfactant solution in deionized water was heated at the same temperature, added to the molten lipid, and mixed at 500 rpm, 85 °C for 10 min using a magnetic stirrer. The hot micro-emulsion was, thereafter, sonicated using a probe-type ultrasonic homogenizer at 60 % amplitude for 10 min. LNPs were obtained via sudden cooling of the nano-emulsion for

5 min. The final volume of the dispersion was adjusted to 10 mL with deionized water. Surfactants/ stabilizers of different types and concentrations were screened for LNPs optimization, Supplementary Table 1A. To prepare the drug loaded LNPs, VRZ was added to the lipid phase during melting.

For DPPC/DMPG-VRZ-LNPs, surface modification was carried out using a thin film hydration method on the pre-synthesized VRZ-LNPs (Jiang et al., 2020). Briefly, 50 mg DPPC mixed with DMPG at different ratios were dissolved in chloroform and methanol mixture (2:1 vol ratio) as shown in Supplementary Table 1**B**. Solvents were evaporated under reduced pressure using a rotary evaporator adjusted at 45 °C and 300 rpm, forming a thin layer on the inner side of a round-bottomed flask. The phospholipid (**PL**) thin film was then hydrated with the developed formulations and left together for 20 min at 45 °C and 300 rpm.

2.3. Physicochemical characterization

The mean particle size (**PS**) and polydispersity index (**PDI**) were determined at 25 °C using Malvern Zeta-sizer NanoZS (**Malvern Instruments, UK**). Dispersions were suitably diluted (1:100) with filtered deionized water to ensure that the light scattering intensity was within the instrument's sensitivity range. Selected formulations were evaluated for zeta potential (**ZP**) at the aforementioned dilution. All samples were measured in triplicates after 2 min sonication. Results were represented as mean value ± standard deviation (**SD**).

Entrapment efficiency (**%EE**) was determined indirectly by measuring the amount of free drug using the centrifugal-ultrafiltration method (El-Melegy et al., 2021). Briefly, 1 mL of the LNPs was placed into the upper chamber of Vivaspin 6 concentrator, 100 K MWCO, and centrifuged for 20 min at 20 °C and 6000 rpm. The concentration of the drug collected in the filtrate was determined by UV spectroscopy at λ_{max} 256 nm. The percentage of entrapment efficiency was calculated according to the following equation.

$$\%EE = \frac{\text{Total amount of drug} - \text{Free drug in aqueous phase}}{\text{Total amount of drug}} \times 100$$

Morphological examination of selected plain or modified formulations was assessed using Transmission electron microscopy (**TEM**) **Jeol, JEM-100 CX electron microscope, Japan**. Diluted samples with filtered deionized water (8:100) were placed on a carbon-copper grid and stained with 2 % Uranyl acetate. After removing the excess solution, the copper grid was set to air-dry before TEM examination.

Fourier Transform Infra-Red spectroscopy **(FTIR)** analyses of the selected formulations and their respective physical mixtures were performed using FTIR spectrometer (**Cary 630, Agilent technologies, USA**) between 750 and 3500 cm^{-1}, to detect any possible interaction between VRZ and lipid components of LNPs. Prior to FTIR, formulations were dried overnight under reduced pressure, 0.1 bar, at −55 °C using LyoQuest freeze drier (**Telstar, Japan**).

Differential scanning calorimetry (DSC) was performed using a DSC TA-60 calorimeter (Shimadzu, Japan). Samples (2–5 mg) were heated in crimped aluminum pans (40–200 °C) at a scanning rate of 10 °C/min. Analyses were carried out under an inert nitrogen purge (35 mL/min), and an empty pan of alumina was used as a reference in each case.

The *in-vitro* drug release profiles of 10 % methanolic VRZ solution, VRZ suspension in 0.5 % w/v carboxymethylcellulose (**CMC),** and the developed VRZ-LNPs (with and without the phospholipid blend) were performed using the dialysis membrane method. Experiments were carried out under sink conditions, 7 times saturated solubility. Dispersions equivalent to 2 mg VRZ were placed into a 24 h pre-soaked VISKING dialysis bag of MWCO 12–14 kDa. The bags were transferred into 15 mL phosphate buffer solution (PBS, pH 7.4) as the release medium in a shaking water bath at 100 strokes/min at 37 °C. At predetermined time intervals, samples (750 µL) were withdrawn from the release medium, replenished with equal volumes of fresh, warm PBS, and then analyzed spectrophotometrically at λ_{max} 256 nm against blank media. The release studies were performed in triplicate and results are presented as the mean value ± SD.

Short-term stability studies were conducted over 3 months of storage at room temperature to investigate the stability of **S7** and DPPC/DMPG surface-modified VRZ-LNPs, **PL^2-S7**, respectively, in terms of colloidal properties and entrapment efficiency. VRZ total content in the developed LNPs dispersion was determined via digesting 50 µL of the LNPs dispersion in 10 mL ethanol: water mixture (50:50) followed by sonication for 10 min at a slightly elevated temperature. The dispersion/ suspension was centrifuged at 6000 rpm for 15 min at room temperature and then the supernatant was filtered through a 0.45 µm syringe filter. A validated HPLC stability-indicating method was utilized for VRZ quantification (Khetre et al., 2009). HPLC analysis was performed using an isocratic system equipped with a reversed-phase C18 column (HC-C18 (2) 150 × 4.6 mm, 5 µm), and a UV detector. The mobile phase consisted of acetonitrile and water in a 40:60 v/v ratio. The flow rate was adjusted at 1 mL/min.

2.4. In-vitro VRZ deposition

The particle deposition pattern is a vital determinant of pulmonary drug delivery success. Anderson cascade impactor **(ACI)** is the principal method for the determination of the particle size distribution emitted from inhaled dry powders. Particle distribution over the 7 stages of the multi-stage cascade impactor can reflect on the respective level of *in vivo* lung deposition following pulmonary administration (Mitchell et al., 2019).

Aqueous dispersions of **S7** and **PL^2-S7** were spray dried using a Buchi, mini-spray dryer (Flawil, Switzerland) using a mixture of carriers (mannitol, maltodextrin, and L-leucine at 1:2:1 w/w ratio). Nanoparticle: carrier mixture was adjusted to 1:4 (w/w ratio) for all spray-dried preparations with 2 % w/v overall solid content. In addition, VRZ aqueous solutions were spray-dried as control. The drying parameters were adjusted to 110 °C inlet temperature, 50 °C outlet temperature, 100 % aspiration rate, 15 % pump rate, and 320 L/h air flow rate. Scanning electron microscopy (JSM-IT200; JEOL, Tokyo, Japan) was used to visualize spray dried formula. Powders were fixed on aluminium stubs and sputter coated with gold at 2 mA for 3 min. Digital images were captured at an accelerating voltage of 10 kV.

For evaluation of the particles aerodynamic performance, 20 mg of each powdered formulation filled in a hard gelatin capsule of size 3 was placed in an Aerosolizer® device coupled via an adaptor to the throat of the Anderson cascade impactor **(ACI)**. The powder was allowed to flow through the impactor operated at 28.3 L/min flow rate. The collection plates were individually and carefully washed with a 1:1 v/v mixture of water and ethanol to collect the particles trapped on each stage. The drug content was quantified by the previously described HPLC method under **section 2.3**. Aerosol deposition performance parameters, mass median aerodynamic diameter **(MMAD)**, geometrical standard deviation **(GSD)**, emitted dose fraction **(EF%)**, and fine particle fraction **(FPF %)** were calculated using Copley Inhaler Data Analysis Software, Inhalytix™ 5000.

2.5. Assessment of antifungal susceptibility

The antifungal susceptibility test **(AFST)** was performed using the broth microdilution standard method (Sanguinetti and Posteraro, 2018) with slight modifications. This was done to determine the minimum inhibitory concentration (**MIC**) of VRZ-LNPs compared to the corresponding free VRZ, against a clinical strain of *A. fumigatus* isolated from sputum samples of leukemia patients diagnosed with IPA. The isolate was obtained from the microbiological stock collection of the Department of Microbiology and Immunology, Faculty of Pharmacy, Alexandria University. Final dilutions of free-VRZ and VRZ-LNPs (with and without DPPC/DMPG) in a range of 0.063–8 µg/mL were prepared and pipetted into the wells of 96-well microtiter plates. Conidial suspensions

in Sabouraud's dextrose broth were added to a final concentration of 5 x 10^4 colony-forming units (CFU)/mL and were gently mixed. The microplates were incubated for 48 h at 37 °C. The MIC endpoints of VRZ were determined visually as the least concentrations of drug providing complete inhibition of fungal growth (clear broth). LNPs; containing the media with the fungal suspension but lacking the drug, served as a positive control (**PC**) whilst a negative control sample **(NC)** contained the media without the drug or the fungus.

2.6. Animal studies

Experimental protocols involving animals were performed according to approval and ethical guidelines of the Institutional Animal Care and Use Committee (IACUC) of Alexandria University (AU 062023226143) and in accordance with the European Parliament Directive 2010/63/EU guidelines for the use of experimental animals. Male Sprague–Dawley rats were used in those studies weighing between 200 and 225 g. They were housed in temperature-controlled rooms with 12 h of light per day and 50 % relative humidity, with free access to food and water.

2.6.1. In-vivo pulmonary VRZ retention studies

To study VRZ lung retention, eighteen healthy Sprague–Dawley male rats were housed in stainless wire mesh cages and fasted overnight with free access to water before treatment. They were randomly divided into 3 groups, each containing 6 animals, as follows:

- **Group A**: VRZ solution in sterile water (1 mg/kg body weight) via IV dose- rat tail vein.
- **Group B**: VRZ dispersion in sterile water (1 mg/kg body weight) via pulmonary administration.
- **Group C: PL^2-S7** (dose equivalent to VRZ-1 mg/kg body weight) via pulmonary administration.

Pulmonary administration was carried out via a non-surgical orotracheal method (Ribeiro et al., 2015). First, rats were anesthetized by intraperitoneal injections of a mixed solution of ketamine (100 mg/kg) and Xylazine (10 mg/kg). Afterward, they were positioned on a frame supported by a board inclined by an angle of around 45°. The mouth was kept open using forceps, and the tongue was held down. In this manner, the vocal cords were visible. Under good illumination, an oral gavage was pushed against the soft palate to enter the trachea. When the tracheal cartilage rings were reached, samples were slowly injected at a dispersion volume of 200 μL (equivalent to 200 μg VRZ).

After administration of the formulations, 3 rats per group for each time interval (1 and 6 h) were sacrificed and subjected to lung dissection (Guillon et al., 2018). Dissected lungs were immediately weighed, homogenized with three-fold volumes of deionized water at 25,000 rpm for 2 min using an IKA high-speed tissue homogenizer. For drug extraction, lung homogenate (**LH**) samples were mixed with an equal volume of acetonitrile containing diazepam (1 μg/mL) as an internal standard. The mixture was vortexed for 1 min, refrigerated for 10 min, and centrifuged at 10,000 rpm and 4 °C for 10 min. Supernatant samples were then withdrawn and filtered using a 0.45 μm syringe filter. For drug quantifications, 100 μL filtered LH samples were injected applying the previously detailed HPLC-UV method under **section 2.3**. However, an additional guard column (ZORBAX, 12.5 × 4.6 mm) was installed to protect the analytical column (HC-C18 (2) 150 × 4.6 mm, 5 μm).

2.6.2. Immunosuppression and neutropenia induction

Induction of immunosuppression was achieved by intraperitoneal injections of cyclophosphamide **Endoxan® Baxter** as previously described (Chandenier et al., 2009; Chauvin et al., 2019). Sprague-Dawley rats (200–225 g) received an initial loading dose of 75 mg/kg cyclophosphamide. This was followed by maintenance doses of 60 mg/kg, given every 4-day interval with a total of 3 doses. All animals were housed individually in clean plastic cages under restricted hygienic conditions. They were fed on a low protein diet with free access to sterile water supplemented with 500 mg/L tetracycline to prevent any undesirable opportunistic bacterial infections and 300 mg/L paracetamol to alleviate pain associated with handling. The adoption of a low protein diet assists in achieving a more reproducible model (Chandenier et al., 2009).

For hematological investigation, orbital sinus blood sampling was performed on six neutropenic rats at predetermined time intervals. Blood was collected into EDTA tubes to obtain complete blood pictures. Rats were systematically weighed and assessed for behavioral changes and/or the development of any hematological or respiratory reactions.

2.6.3. A. Fumigatus infection

2.6.3.1. Route of inoculation. The fungi were cultured on Sabouraud's dextrose agar at 37 °C for 2 days and the conidia were harvested with saline moistened swabs and resuspended in sterile saline. Quantitative counts were conducted to calculate the dilution to achieve the target inoculum size. Several routes of infection have been described to induce experimental pulmonary aspergillosis in animal models (Desoubeaux and Cray, 2018). Among these, the intranasal, orotracheal, and intratracheal inoculation were explored in attempts to recapitulate the disease's natural pathophysiology. Nine neutropenic male Sprague Dawley rats were randomly distributed into three groups with different inoculation methods (**groups I, II, III).** The rats were challenged with a mean inoculum size of 5 × 10^7 CFU/dose, one day after the first cyclophosphamide maintenance dose (D_0; the day of experimental infection). Intranasal deposition **(Group I)** was performed via instilling the conidial suspension into the rat's nares, while oral-endotracheal **(Group II)** was done via direct placing of the conidial suspension into the top of the trachea using an oral gavage. Intratracheal instillations **(Group III)** of the conidial suspension were administered directly into the bottom of the trachea through a tracheotomy.

For confirmation and quantification of the induced infection, the inoculated rats were sacrificed 48 h post-infection as the mycelial growth is known to be firmly established after 30 h in neutropenic rodents (Habicht et al., 2002). Lungs were collected in 5 mL sterile saline, homogenized, and plated. Plates were incubated at 37 °C for 24 and 36 h, after which the *Aspergillus* burden in terms of CFU/lung was determined. Careful aseptic surgeries were performed to avoid bacterial or fungal contaminations.

2.6.3.2. Inoculum size. For determination of the appropriate inoculum size, nine neutropenic male Sprague Dawley rats were randomly distributed into three groups **(IV, V, and VI).** Each group of them was anesthetized using an intraperitoneal mixed injection of ketamine (100 mg/kg) and xylazine (10 mg/kg) then challenged with a different infection dose via intratracheal installation directly to the bottom of the trachea using surgical tracheotomy (Ghali, 2018; Ribeiro et al., 2015). On D_0, a 100 μL spores aliquot from each dilution, was applied directly into rats' trachea providing three different total inoculum doses; 5 × 10^6 **(Group IV)**, 5 × 10^5 **(Group V)** and 5 × 10^4 **(Group VI)** CFU, respectively. After the procedure, the skin and the adjacent subcutaneous tissues were sutured back aseptically. *Aspergillus* burden in terms of CFU/lung was determined as described in **section 2.6.3.1.**

2.6.4. Experimental design and treatment protocol

The previously described animal model of IPA in neutropenic rodents (Chauvin et al., 2019) was adopted and optimized with slight modifications as shown in Fig. 1. In brief, neutropenia was induced by the intraperitoneal administration of 75 mg/kg cyclophosphamide 5 days before fungal inoculation ($\mathbf{D_{-5}}$). This was followed by the administration of 3 maintenance doses of 60 mg/kg; one day before inoculation ($\mathbf{D_{-1}}$), on ($\mathbf{D_3}$), and ($\mathbf{D_7}$), after fungal inoculation, respectively. Forty-two male Sprague–Dawley rats were allocated randomly into four different groups

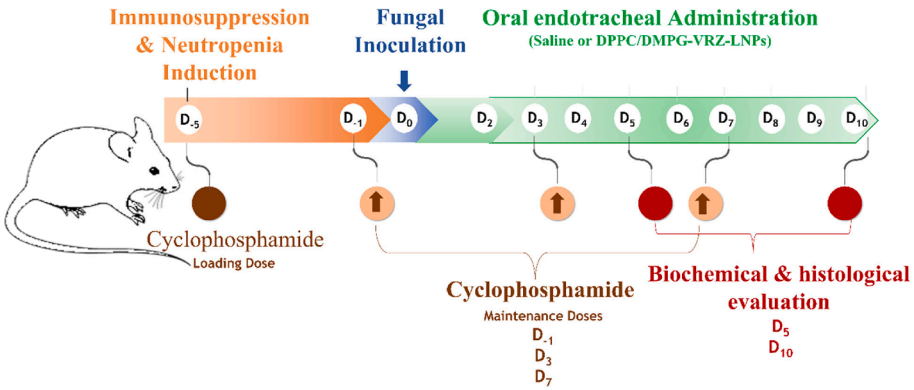

Fig. 1. Schematic representation of experimental induction of invasive pulmonary aspergillosis (IPA) in a neutropenic rat model. Aspergillus Fumigatus fungal load of 5×10^6 CFU/100 μL was administered via intratracheal instillation at D_0. A treatment plan using daily DPPC/DMPG-VRZ-LNPs PL^2-S7 dispersion (1 mg VRZ/Kg body weight) via oral endotracheal administration was adopted.

as detailed in Table 1.

Fungal spores: 5×10^6 CFU dispersed in 100 μL sterile saline, were administered using intratracheal instillation under general anesthesia as stated in **section 2.6.1.** Treatment started 48 h after fungal inoculation (**D_2**), a time point at which the fungal growth was confirmed by mycelial count. DPPC/DMPG surface-modified-LNPs (**PL^2-S7**) were administered non-surgically through an oral endotracheal instillation of an oral gavage under good illumination to visualize the trachea. Treatment was received daily **(D_2 to D_9)**. The treatment regimens included 1 mg VRZ/kg/day. Control neutropenic rat groups: either uninfected or infected **(UN or IN)**, received saline instead of VRZ LNPs.

2.6.5. *Survival and clinical manifestations*

A common limitation of pulmonary aspergillosis animal models is the inability to make an early assessment to measure the impact of the administered treatment (Kirkpatrick et al., 2013). The survival of the infected rats was monitored daily, and the mortality was recorded up to 10 days post-infection. Animals removed at sacrifice (n = 3 per time point) were considered as censored deaths. After which, surviving rats were humanely sacrificed.

IPA rodent model is often associated with marked body weight loss as the disease is frequently accompanied by nutritional problems (Chandenier et al., 2009). Monitoring clinical signs including rats' body weight and respiratory function, started from the second day after experimental inoculation when clinical status began to deteriorate. Reduction in body weight ≥ 20 % of the baseline (weight on D_0) was considered a vital marker for severe infection (Desoubeaux and Chandenier, 2012). Respiratory wheezing is defined as an audible breathing sound, mostly a squeaking sound associated with a rapid respiratory rate. It is considered as clinical evidence of severe pulmonary disease (Desoubeaux and Chandenier, 2012).

2.6.6. *Biochemical and histopathological analyses*

Biochemical assessment of the fungal burden in rats' lungs was performed by quantitative detection of *A. fumigatus* galactomannan **(GM)** antigen concentration in bronchoalveolar lavage fluid **(BALF)** specimens via enzyme-linked immunosorbent assay **(ELISA)** (Arastehfar et al., 2021; Freeman Weiss et al., 2021). GM is a fungal cell wall polysaccharide that can be released by *Aspergillus* species during growth starting from the early stages of the infection (Osibe et al., 2020). Briefly, at predetermined time intervals (D_5 and D_{10}; Fig. 1), BALF samples were collected via exposure and catheterization of the tracheas, under general anaesthesia. A 24G catheter was carefully inserted into the middle of the trachea between two cartilage rings and stabilized by tying the trachea around it. Afterward, 3 mL sterile saline was gently injected into the lung and aspirated 3 successive times. BALF samples were then collected in sterile falcons and centrifuged for 10 min at 10,000 rpm and 4 °C to collect the supernatant. The supernatants were stored at −20 °C for subsequent analysis. The BALF-GM concentrations were measured in Mabaret El-Asafra Labs, Alexandria, Egypt, using a Dynamiker Aspergillus Galactomannan Assay Kit (Dynamiker Biotechnology, Tianjin).

Histopathological examination is considered the gold standard for diagnosis and quantification of IPA. Moreover, it allows the exclusion of another diagnosis such as malignancies and non-fungal pulmonary infections (Stolz et al., 2018). Segments of the lungs from some selected animals were fixed in 10 % phosphate-buffered formalin, pH 7.4, and stored at room temperature for histopathological analyses. In brief, two sagittal macroscopic cross sections were dehydrated in graded ethanol (70–100 %), cleared in xylene, and then paraffin-embedded. After that, paraffin-embedded tissue sections were sectioned into 5 μm thick slices using a microtome. After mounting, the slides were de-waxed in xylene, hydrated using graded ethanol, stained with either hematoxylin–eosin–saffron (**HES**) or periodic acid Schiff (**PAS**), and examined under a light microscope.

2.7. *Statistical analysis*

Statistical data analysis was carried out using either one- or two-way analysis of variance test (ANOVA) followed by Tukey's multiple comparisons post-hoc tests using GraphPad Prism Software, Version 9.5.1. Differences were considered statistically significant at p-values < 0.05.

Table 1
Induction of experimental invasive pulmonary aspergillosis in a neutropenic rat model and subsequent treatment protocol using daily oral endotracheal administration of PL^2-S7 dispersion (1 mg VRZ/Kg body weight).

Animal Group	Codes	Specifications		
		No. of animals per group	*A. fumigatus* Infection	Treatment
Uninfected/Non-Treated	UN	6	–	Saline
Uninfected/Treated	UT			PL^2-S7 LNPs
Infected/Non-Treated	IN	15	5×10^6 CFU/100 μL	Saline
Infected/Treated	IT			PL^2-S7 LNPs

3. Results and discussion

3.1. VRZ and DPPC/DMPG surface-modified VRZ LNPs properties

3.1.1. Colloidal properties and entrapment efficiency

Different stabilizers were scrutinized for LNPs stabilization. Results revealed that the type and concentration of the stabilizer had remarkable effects on the physicochemical properties of LNPs. Among these, PLX 407 (**S6**), Table 2**A,** yielded nanoparticles of hydrodynamic diameters ≤ 200 nm and PDI ≤ 0.2 in comparison to PLX 188 (**S4**), tween 80 (**S2**) and PVA (**S10**), which displayed larger hydrodynamic diameters with higher polydispersity at the same concentration, 1 % w/v. Nanoparticles with a diameter less than 200 nm have been reported to have a greater chance of mucus penetration, avoid clearance by macrophages, and are efficiently capable of reaching the alveoli (Deng et al., 2021). Increasing the stabilizer concentrations from 0.5 % to 1 % w/v decreased the nanoparticles' size, apart from PVA-stabilized LNPs, **S9,** and **S10**, which exhibited a significant increase in particle size and PDI. This could be attributed to the stabilizing ability rather than the emulsifying potential of PVA (Turk et al., 2014).

The developed LNPs (**S6;** Compritol nanoparticles stabilized with 1 % w/v PLX 407) exhibited negative surface charge (-28.7 ± 1.20 mV) because of the ionization of glyceryl behenate, a fatty acid composing Compritol® (Khan et al., 2018). The higher the ZP value, the higher the repulsion forces between the particles are, and accordingly, the tendency of physical instability via aggregation is minimized.

VRZ-loaded LNPs; **S7** didn't significantly alter the colloidal properties of the plain LNPs**,** Table 2**A.** This could be attributed to VRZ (pKa 1.76) availability in the non-ionizable state that guaranteed its solubility in the lipid phase. However, when the drug concentration increased to 0.15 % w/v, **S8,** drug crystals were observed**,** indicating that 0.1 % w/v is the optimum drug concentration capable of providing stable VRZ-LNPs: **S7**, with (60.15 ± 3.3 %) EE. In a similar fashion, previous studies report no changes in nanoparticle size with drug load up to 0.2 %. However, a 50 % particle size increase was observed upon increasing drug load from 0.2 to 1 % and drug precipitation can be observed beyond this level (Krishnamachari et al., 2007; Sharma et al., 2016).

Being a neutral phospholipid, DPPC adsorption on the VRZ-LNPs surface was anticipated to reduce the negative zeta potential value. As shown in Table 2**B and** Supplementary Fig. 1, a reduction in the surface charge of PL-S7 was observed, in an indication of phospholipid surface localization. An increase in nanoparticle size was also observed coupled

Table 2
Composition and physicochemical properties of (A) plain and VRZ-loaded LNPs with different types and concentrations of stabilizers, (B) DPPC/DMPG surface-modified VRZ-loaded LNPs at different DPPC: DMPG ratios.

Codes	Stabilizer (% w/v)		VRZ (%w/v)	Colloidal properties			EE % A
				PS (nm) ±SD	PDI ±SD	ZP (mV)	
S1	Tween 80	**0.5**	-	308.6 ±3.57	0.242 ±0.013		
S2		**1**	-	238.8 ±1.82	0.235 ±0.235		
S3	PLX 188	**0.5**	-	325.0 ±4.37	0.367 ±0.021		
S4		**1**	-	297.7 ±6.22	0.456 ±0.140		
S5	PLX 407	**0.5**	-	335.0 ±5.51	0.357 ±0.013		
S6		**1**	-	190.2 ±2.55	0.148 ±0.012	-28.7 ±1.20	
S7			**0.10**	193.6 ±3.48	0.178 ±0.014	-27.9 ±0.65	60.15 ±3.30
S8			**0.15**	**Drug precipitation**			
S9	PVA	**0.5**	-	693.5 ±11.74	0.284 ±0.286		
S10		**1**	-	900.9 ±65.16	0.436 ±0.121		

Codes	PL-Mixture		Colloidal properties			EE% B
			PS (nm) ±SD	PDI ±SD	ZP (mV) ±SD	
S7	-		193.6 ± 3.48	0.178 ± 0.014	-27.9 ± 0.65	60.15 ± 3.31
PL-S7	DPPC: DMPG	**1:0**	243.3 ± 24.73	0.350 ± 0.023	-14.5 ± 2.05	83.91 ± 1.20
PL^1-S7		**4:1**	200.9 ± 3.31	0.265 ± 0.011	-59.4 ± 8.90	59.85 ± 1.38
PL^2-S7		**9:1**	220.6 ± 2.60	0.271 ± 0.025	-42.4 ± 2.30	80.81 ± 0.76
PL^3-S7		**19:1**	227.0 ±7.28	0.280 ±0.020	-41.5 ±1.93	85.64 ±1.15

with remarkable enhancement in VRZ entrapment efficiency. However, PL-S7 revealed poor colloidal stability with an increased risk of coalescence upon storage, compared to the unmodified counterpart.

Phospholipid-stabilized LNPs could exhibit aggregation or gelling behavior upon storage. Triglyceride crystallization alters the dispersed phase, increasing the specific surface area and disrupting the phospholipid surface coverage. Such uncovered surfaces promote LNPs aggregation (McClements and Jafari, 2018). Another theory from the lung physiology point of view, suggests that packaging and adsorption of pure DPPC layer into interfaces may introduce surface stiffness (Veldhuizen et al., 1998). Accordingly, co-surfactant inclusion may improve the coverage of the bare lipid surface to prevent possible aggregation (Pichot et al., 2013). From these perspectives, mixing DPPC with fluid-acidic phospholipids: phosphatidylglycerol, and phosphatidylinositol representing 8–15 % of the total phospholipid lung surfactant pool (Veldhuizen et al., 1998), might lead to adsorption enhancement on LNPs surfaces as they play a crucial role in surface tension reduction.

Dimyristoyl-phosphatidylglycerol DMPG was investigated as an adsorption enhancer for DPPC surface coating at three different ratios as shown in Table 2**B.** The inclusion of DMPG maintained nanoparticles' stability, mono-dispersibility, and reproducibility (**Supplementary** Fig. 1D, **E).** LNPs surface charge was sensitive to the DPPC/DMPG blend ratios indicating that the phospholipids were adsorbed on the surface of the LNPs. Increasing DMPG concentration in the adsorbed DPPC film was associated with a reduction in nanoparticle size and a noticeable increase in the negative ZP compared to DMPG-free DPPC surface-modified formulation; **PL-S7**. To attain stable yet efficient, non-toxic nanoparticles for pulmonary administration, DMPG concentration was reduced to achieve a negative surface charge capable of maintaining the system stability (DPPC: DMPG 9:1).

Regarding VRZ entrapment efficiency **(EE%),** DPPC-surface modification resulted in a significant increase ($p = 0.0006$) in the entrapment efficiency of 83.91 ± 1.2 % compared to 60.15 ± 3.31 % for **S7,** Table 2**B**. Upon DMPG addition at 20 % w/w of PL mixture, **PL^1-S7,** a considerable decline in the entrapment efficiency was observed. This can be attributed to the increased fluidity of the DPPC shell upon mixing with DMPG or to the increased VRZ aqueous solubility prompted by DMPG acidity. Gradual reduction in DMPG proportions of the PL mixture down to 10 and 5 % w/w in **PL^2-S7** and **PL^3-S7** respectively, retained the high value of entrapment efficiency observed for DMPG-

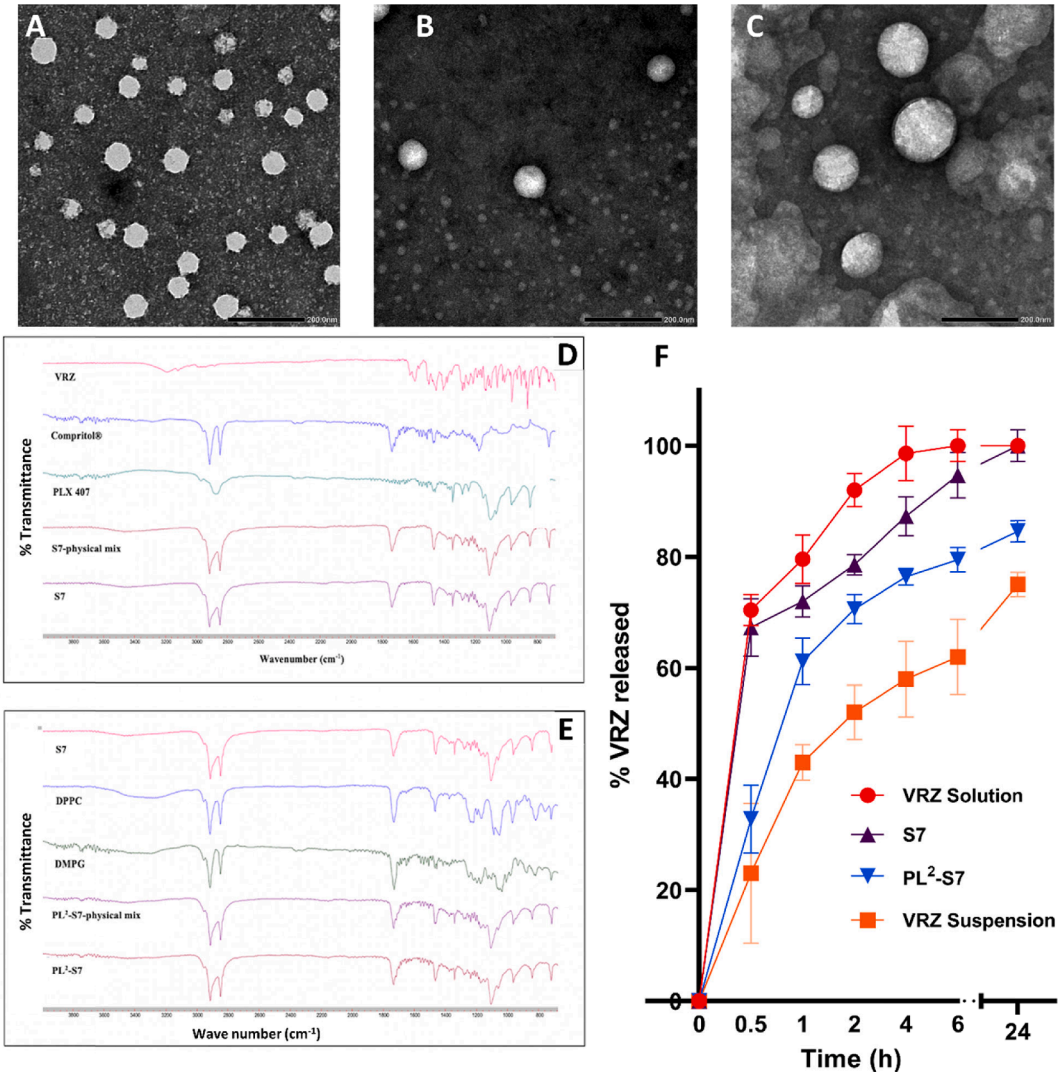

Fig. 2. *In vitro* characterization of VRZ-LNPs (A-F). Transmission electron micrographs (TEM) of Compritol LNPs (A-C); plain LNPs S6, 148.31 ± 21.09 nm (A), VRZ-LNPs S7, 79.54 ± 7.56 nm (B), and DPPC/DMPG surface-modified VRZ-LNPs, PL^2-S7, 123.06 ± 24.03 nm (C), scale bar 200 nm. Fourier Transform Infra-Red spectra of the selected VRZ-LNPs (D, E); S7 (D), and PL^2-S7 (E), with their respective components and physical mixtures. (F) *In-vitro* release profiles of VRZ from methanolic solution, 0.5 % w/v CMC suspension, and selected VRZ-LNPs formulations; S7 and PL^2-S7 through a dialysis membrane at 37 °C in PBS, pH 7.4.

free formulation **PL-S7** with no significant differences, Table 2**B**.

3.1.2. TEM and FTIR

TEM studies were conducted to investigate the optimized LNPs morphology and size. As shown in Fig. 2**A–C,** LNPs were spherical, smooth-surfaced nanoparticles with quite uniform particle size distribution. Moreover, VRZ loading didn't alter the nanoparticle size or morphology. The size determined by TEM imaging was smaller than that measured by dynamic light scattering (DLS). Transmission microscopy yields an average number for the diameter size of the particle core, while DLS measures the hydrodynamic diameters that reflect how the particles diffuse within a fluid. Upon examination of DPPC/DMPG surface-modified formulation; **PL^2-S7** (Fig. 2**C),** TEM imaging revealed a slight increase in particle size compared to DPPC-free formulation; **S7** (Fig. 2**B)** which comes in good agreement with the results of dynamic light scattering. Notably, TEM imaging couldn't aid in the visualization of the adsorbed PL film. However, better sphericity and less corrugated surfaces were detected for PL-containing formulations, especially **PL^2-S7.** This could be attributed to the conjugated PL surface activity, confirming the proper adsorption of the PL film onto the particles.

As shown in Fig. 2**D, E**, the FTIR spectrum of VRZ exhibited characteristic peaks, C-O stretching at 1127 cm^{-1}, O–H stretching at 3190 cm^{-1} aromatic bonding vibration at 958 cm^{-1}, 857 cm^{-1}, 663 cm^{-1}, C–C aromatic stretching band at 1586 cm^{-1} and 1617 cm^{-1}, C-N stretching at 1277 cm^{-1}. For lipid excipients, Compritol®, DPPC, and DMPG, characteristic C–H stretching bands of long fatty acid chains at 2920 cm^{-1} and 2850 cm^{-1} were identified in addition to a C=O stretching band at 1734 cm^{-1}. Furthermore, P=O and P-O-C stretching bands were observed at 1237 cm^{-1} and 1052 cm^{-1} respectively for DPPC and DMPG-containing formulations. DPPC also exhibited a characteristic $N^+(CH3)_3$ stretching band at 974 cm^{-1}. Physical mixtures showed summations of the vibrational frequencies of the individual components suggesting the absence of recrystallization and/or interaction between auxiliary materials during processing. In the FTIR spectrum of the VRZ-LNPs, both the aromatic bonding vibration and O–H stretching of VRZ were decreased but did not disappear. This behavior suggests that the chemical structure of VRZ had not changed after entrapment within the developed LNPs.

3.1.3. In-vitro VRZ release

The *in-vitro* release profiles for the selected VRZ-loaded formulations (**S7 and PL^2-S7)** in addition to VRZ solution in 10 % w/v methanol and VRZ suspension in 0.5 % CMC are shown in **(**Fig. 2**F)** Drug release media consisted of 15 mL PBS, pH 7.4 at 37 °C which provide sink condition for 2 mg VRZ (saturation solubility was 0.934 ± 0.007 mg/mL) using dialysis bag method. About 80 % of the free drug was released after 1 h in case of control solution confirming proper dialysis-ability. For suspension, the drug release showed a biphasic behavior with an initial rapid release of about 60 % VRZ in 6 h followed by a sustained slower phase within the next hours resulting in 75 % of drug release over 24 h.

VRZ incorporation into LNPs in amorphous form as confirmed by DSC (**Supplementary** Fig. 2) resulted in an enhancement in drug dissolution associated with rapid onset of action. For pulmonary drug delivery, the rapid onset of drug release is favorable since the drug is directly targeted toward its local site of action. Inhaled therapeutics should have fast onset of action especially with infectious lung diseases or upon vaccination (He et al., 2022). For DPPC-free LNPs, **S7,** an initial high burst release was observed, nearly 70 % of the entrapped drug was released after 1 h. This remarkable enhancement in drug dissolution can be attributed to the high surface area of the nanosized LNPs, in addition to possible drug localization near the particle surface within the surfactant polar shell rather than in the lipid matrix core (Kwok and Chan, 2014).

Tracheobronchial airways are cleared of deposited particulates within 24 h (Newman, 2017). Accordingly, inhaled therapy should provide a rapid onset of action followed by a sustained release phase within this time frame. DPPC/DMPG surface-modified formula, **PL^2-S7**, VRZ was released in a slowly sustained manner over 24 h in comparison to the phospholipid-free LNPs, **S7**, which showed a fast burst release. Such a sustained manner could be attributed to the slow diffusion of VRZ across the phospholipid coat layer (Li et al., 2020). In addition to DPPC surface modifying capability to prevent immune system recognition by the macrophages, it may aid in sustaining VRZ release to avoid rapid systemic absorption. Hence, the developed DPPC/DMPGsurface-modified LNPs can be potential bioactive nanocarriers in controlling VRZ release in the treatment and prophylaxis of IPA.

3.1.4. Storage stability

A validated HPLC method was utilized for the quantitative determination of VRZ at the predetermined time intervals (Khetre et al., 2009). VRZ peak was eluted at 6.49 min as shown in **Supplementary** Fig. 3A. VRZ calibration curve at 25 °C using 20 μL injection volume showed linearity with an excellent correlation coefficient over 5–25 μg/mL VRZ (**Supplementary** Fig. 3**B**). The stability of the selected formulations was evaluated in terms of particle size, PDI, ZP, and EE% at 0, 15, 45, and 90 days upon storage at room temperature. As shown in Fig. 3, DPPC/DMPG-free formulation, **S7,** showed a non-significant change in either particle size or PDI after 15 days of storage. However, it exhibited a significant decrease in EE% over the 15-day interval followed by eventual VRZ expulsion and observation of suspended drug crystals at later time points. These results can be aligned with our loading studies, confirming the limited capabilities of the plain LNPs for VRZ encapsulation in comparison to DPPC/DMPGsurface-modified formulations.

On the other hand, **PL^2-S7** showed a reduction in particle size and negative ZP after 15- and 45-day intervals. This can be attributed to the possible mobility of the phospholipid film to be embedded within the particles with time to reduce particle size with slight masking of DMPG-induced negative charge. At D90, a gradual increase in particle size and negative zeta potential was observed. This could be attributed to the possible DPPC layer shedding with slight reversion to the higher negative surface charge resulting from either DMPG surface deposition or fatty acid hydrolysis. DPPC/DMPG-surface modification provided a very promising strategy in maintaining VRZ-LNPs stable in the dispersion without any drug expulsion or change in EE% even after 90 days. Accordingly, the developed surface-modified VRZ-LNPs (**PL^2-S7)** endowed an additional merit as a candidate nanocarrier system for pulmonary VRZ delivery preserving drug content upon storage.

3.2. In-vitro VRZ deposition

DPPC/DMPGsurface-modified LNPs, **PL^2-S7** showed a desirable particle deposition pattern with acceptable aerodynamic parameters, Fig. 4**A & B**. Higher percentages of VRZ were recovered from stages 4, 5, and 6 representing secondary and terminal bronchi and alveolar ducts respectively. Surface modification of LNPs decreased the mass median aerodynamic diameter value, MMAD 3.20 μm vs 4.77 μm for the unmodified **S7** indicating a higher probability of depositing deep into the lung. This was supported by SEM and flow properties **(Supplementary** Fig. 4**)** that showed powder stickiness for spray-dried **S7**. Such stickiness resulted in individual particle aggregation and the formation of large agglomerates unable to be aerosolized**.** Moreover, DPPC/DMPG -surface modification resulted in a significant increase in EF% and FPF% values. As shown in Fig. 4**B**, spray-dried **PL^2-S7** displayed EF% and FPF% values of 84.32 and 71.44 respectively, compared to 63.51 and 43.28 for spray-dried **S7**. High percentages of emitted dose fraction and fine particle fraction indicate improved aerosolization performance which, in turn, will guarantee deep lung deposition. Our results are in accordance with Ishak and Osman who reported that the use of phospholipids, the main component of lung surfactants during spray drying, improved particle migration to the lung periphery (Ishak and Osman, 2015).

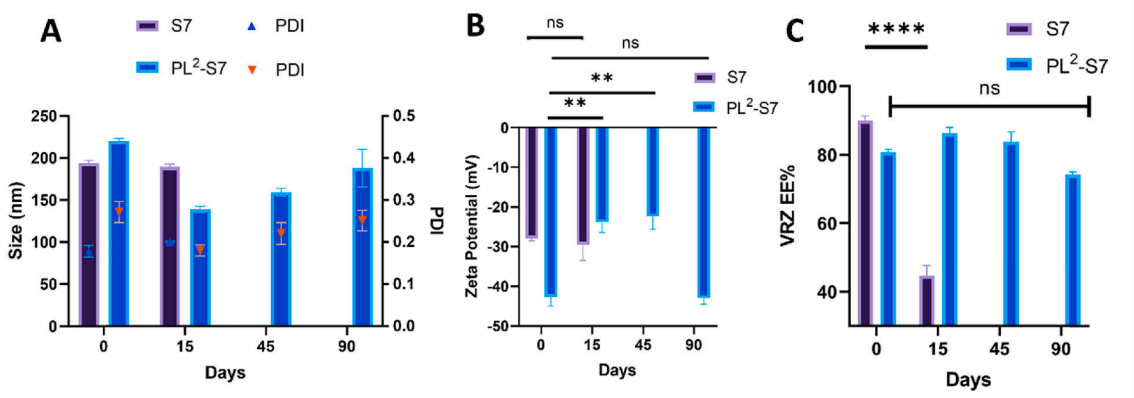

Fig. 3. Colloidal properties of VRZ-loaded LNPs-S7 and DPPC/DMPG surface-modified VRZ LNPs, PL^2-S7 over 90 days storage at room temperature. Hydrodynamic diameters and PDI as determined by dynamic light scattering (A), Zeta potential measurements (B), and VRZ EE% (C). (N = 3 and bars are S.D.) Two-way ANOVA followed by Tukey's multiple comparisons. Data were considered significant at $p < 0.05$.

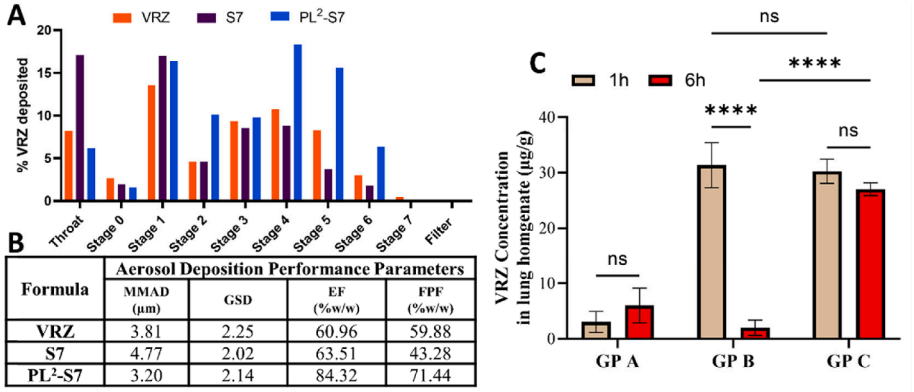

B

Formula	Aerosol Deposition Performance Parameters			
	MMAD (µm)	GSD	EF (%w/w)	FPF (%w/w)
VRZ	3.81	2.25	60.96	59.88
S7	4.77	2.02	63.51	43.28
PL^2-S7	3.20	2.14	84.32	71.44

Fig. 4. VRZ lung deposition. A. In-vitro deposition of spray-dried VRZ containing microparticles (VRZ, S7, and PL^2-S7) determined using Anderson Cascade Impactor operated at 28.3 L/min flow rate (n = 1). % VRZ deposited at each stage was quantified using HPLC. B. Aerosol deposition performance parameters of spray dried VRZ loaded formulations as determined by Copley Inhaler Data Analysis Software, Inhalytix™ 5000. C. In-vivo lung retention of VRZ in healthy male Sprague Dawley rats following IV or pulmonary administration. VRZ in rats' lung homogenates were measured 1 and 6 h after administration of a single dose of VRZ, 1 mg/kg body weight; IV (GP A) or intrapulmonary (GP B; VRZ dispersion and GP C; PL^2-S7). Data represents mean ± SD, (n = 3 for each time point). Two-way ANOVA followed by Tukey's multiple comparisons, $p < 0.05$ is considered significant.

Table 3
Tabular representation of the microbroth dilution method for the determination of MIC values (VRZ µg/mL) at 48 h of both VRZ solution and LNPs against *Aspergillus fumigatus* clinical isolate (5 x 10^4) colony forming units (CFU)/mL. Blank LNPs were included in serial dilutions matching their VRZ-LNPs counterparts.

Test samples	MIC (µg/mL)							
	8	4	2	1	0.5	0.25	0.125	0.063
Blank LNPs[1]	+	+	+	+	+	+	+	+
VRZ Solution	–	–	–	–	–	+	+	+
S7	–	–	–	–	–	+	+	+
PL^2-S7	–	–	–	–	–	+	+	+
Control Samples	**Observed Cultures**							
PC[2]	+							
NC[3]	–							

(-) Clear broth, (+) Turbid broth.
MIC values are shaded in grey.
[1] Blank LNPs: VRZ-free LNPs.
[2] PC: positive control containing broth media with fungal suspension without VRZ.
[3] NC: negative control containing broth media without VRZ or fungal suspension.

3.3. Antifungal susceptibility

The antifungal activities of the free VRZ solution and the developed VRZ-LNPs; **S7 and PL^2-S7,** were recorded after 48 h of incubation using the broth microdilution method (Sanguinetti and Posteraro, 2018). It is worth mentioning that the cultured Aspergillus strain was a slow-growing isolate, making MICs reading after 24 h unreliable, and hence the method was slightly modified to measure MIC after 48 h. It must be noted that no difference in MIC values was observed between different VRZ formulations, Table 3. This could be possibly explained by the equal capabilities of both systems to release > 80 % of VRZ within 24 h (Fig. 2**F**). VRZ control solution and loaded LNPs, with and without DPPC/DMPG, showed an MIC value of 0.5 µg/mL suggestive of drug availability from LNPs without compromising its *in-vitro* antifungal capabilities.

3.4. Animal studies

3.4.1. In-vivo pulmonary VRZ retention

The chromatographic conditions utilized for HPLC determination of VRZ concentration during the short-term stability study (**section 2.3**) were adopted for the *in-vivo* evaluation. However, the injection volume was increased to 100 µL and a guard column was installed between the injector and the analytical column for analysis of biological samples.

Minor changes in retention times and the overall run time were observed. The calibration curve of peak ratio versus time of VRZ (range: 0.2–1 μg/mL) spiked with 1 μg/mL diazepam as an internal standard in rat lung tissue homogenate revealed linearity with a coefficient of determination value of 0.999. The limit of detection (LOD) and limit of quantitation (LOQ) were 0.028 and 0.085 μg/mL, respectively. The intra-day precision and inter-day precision were 2.4 % and 3.7 %, respectively. The recovery percentage ranged from 99.04 % to 101.34 %.

Deposition and absorption profiles of drugs administrated via the pulmonary route should be carefully evaluated. It provides information relevant to the amount of drug available locally to produce a therapeutic effect in the lungs and the overall systemic exposure (Borghardt et al., 2018). Accordingly, this experiment was carried out to estimate the amount of VRZ retained in the lungs after pulmonary administration of **PL^2-S7,** in comparison to crude VRZ dispersed in sterile water. For further comparison, drug amounts in the lungs after intravenous administration of VRZ solution as, as well, investigated.

Different sample types can be collected to quantify drug concentration in the lung such as BALF, sputum, and lung tissue homogenates (Sou et al., 2019). Among them, BALF and sputum samples are more likely to represent the extracellular concentration of the drug, meanwhile, lung micro-dialysis samples are more likely to reflect drug amounts at a particular site of the lung tissue. On the contrary, lung homogenates **(LH)** help in providing an overall estimation of total drug concentration in the lung; including both intracellular and extracellular compartments (Sou et al., 2019). From these perspectives, amounts of VRZ in LH described as VRZ amount (μg) per lung weight in grams were measured at 1 and 6 h (Fig. 4**C**). After one hour, VRZ concentration was significantly lower ($p < 0.0001$) for IV-VRZ (**GP A**, 3.03 ± 1.89 μg/g) than for pulmonary administrated; **GP B and C** (31.35 ± 4.07 and 30.25 ± 2.21 μg/g) respectively. Interestingly, at the six-hour interval after the IV bolus dose; GP A, a considerable, yet non-significant, increase was observed (6.3 ± 3.14 μg/g). However, with intrapulmonary administration, a rapid decline in drug concentration was observed in the case of free VRZ dispersion (**GP B**, 2.7 ± 1.35 vs 31.35 ± 4.07 μg/g). This result can be aligned with the previously published data which explained the poor local pharmacological effect of inhaled VRZ as a result of rapid absorption into the systemic circulation (Merlos et al., 2014). On the other hand, VRZ loaded in LNPs, **PL^2-S7**, maintained high local drug concentration in LH samples (27 ± 1.14 μg/g) after 6 h.

Higher pulmonary drug concentrations can often be achieved via enhanced peripheral deposition with mucociliary movement back to the trachea-bronchial region. This can be achieved via formulating drug-loaded nanoparticles with particle size less than 500 nm which escape the mucociliary clearance and displace the particles to the airway epithelium (Mangal et al., 2017). It was reported by Bhavna *et al.* that an increased interaction of nano-salbutamol with the lung membrane was achieved when compared to micronized drug (Kumar et al., 2008). This increased interaction of drug-loaded nanoparticles with the lung membrane may increase the residence time of the drug in the lung leading to improvement in the pharmacokinetic parameters and thus the therapeutic index. The significant lung localization achieved by DPPC/DMPG-VRZ-LNPs can be attributed to particle size, formula composition, and release kinetics. Encapsulating VRZ into surface-modified LNPs assisted in sustaining drug release which in turn resulted in higher lung retainment and prolonged residence times. Moreover, the integration of DPPC/DMPG assisted in the production of free-flowing dry powder. To sum up, the main finding of this study is that DPPC/DMPG surface-modified VRZ-LNPs; (**PL^2-S7, GP C),** can be a very successful bio-inspired platform for pulmonary administration of VRZ.

3.4.2. *Immunosuppression and neutropenia induction*

During preliminary investigations, corticosteroids-induced immunomodulation was investigated in a dosing regimen as previously reported (Lo Giudice et al., 2010). Although it showed lower mortality compared to the neutropenic/cyclophosphamide-based approach adopted in the current study, poor reproducibility regarding the disease induction, severity, and progress, was observed (data not shown). As demonstrated in Table 4**,** cyclophosphamide treatment resulted in overall deterioration in the blood picture with a remarkable reduction in total blood leukocyte counts (WBCs < 1 × 10^3/μL) 4 days after the cyclophosphamide loading dose **(D_{-2})**. However, neutropenia was observed one day after the first maintenance dose which matches the day of fungal inoculation, D_0 (Fig. 1**)**. This reduction persisted during the treatment period.

No spontaneous death was observed during the 10-day post-cyclophosphamide treatment. The adopted doses did not exacerbate

Table 4
Induction of immunosuppression and neutropenia using Cyclophosphamide; 75 mg/kg loading dose and 60 mg/kg maintenance doses, on hematological parameters of male Sprague Dawley albino rats, n = 6, over 10-day period. The top panel shows the animal study timeline relevant to the chronological complete blood picture.

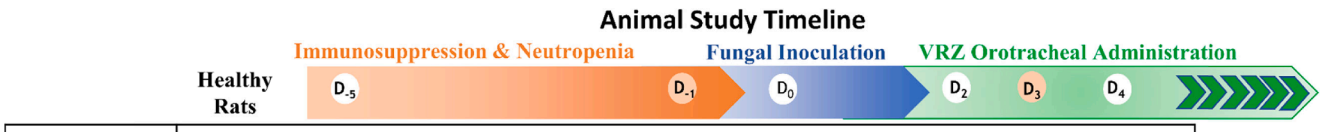

Hematological parameters	Time intervals (Days)										
	D_{-6}	D_{-5}	D_{-4}	D_{-3}	D_{-2}	D_{-1}	D_0	D_1	D_2	D_3	D_4
WBCs (×10^3/ μL)	5.7 ±2.35	Cyclophosphamide Loading dose			0.6 ±0.48	Cyclophosphamide Maintenance Dose	0.47 ±0.33			Cyclophosphamide Maintenance Dose	0.466 ±0.47
Lymphocytes (%)	76.25 ±3.4				78.75 ±5.9		89.5 ±2.38				85.33 ±5.8
Neutrophils (%)	14.75 ±3.09				15.25 ±3.4		5.5 ±1.29				5 ±1
Monocytes (%)	5.75 ±1.7				4.25 ±0.95		3.25 ±1.25				4.33 ±1.15
Eosinophils (%)	3.25 ±1.25				3.25 ±1.7		2.25 ±1.25				2.33 ±1.5
HB (g/dL)	14.2 ±0.6				12.42 ±0.6		9.55 ±0.77				8.96 ±2.2
RBCs (×10^6/ μL)	6.35 ±0.42				5.73 ±0.33		4.33 ±0.35				3.9 ±2.2
HCT %	43.02 ±2.69				38.15 ±3.32		26 ±2.52				23.4 ±5.9
Platelets (×10^3/ μL)	653.5 ±39.04				599 ±48.15		244.75 ±32.73				16 ±3.6

the mortality. However, after the second cyclophosphamide maintenance dose, nose bleeding, a sign of hematological disorder, was observed in ~ 15 % of the rats. This can be aligned with the observed significant reduction in the mean platelet count. Cyclophosphamide elicited severe thrombocytopenia at days zero and 4 in the experimental immunosuppression and establishment of fungal infection, with a drastic decrease down to 95 % from the normal baseline at D_4. This comes in agreement with previous studies on the induction of thrombocytopenia in rodents using cyclophosphamide (Nandini et al., 2021) where a noticeable drop in platelet counts was observed on the 6th day of cyclophosphamide treatment.

Regarding the clinical status, a slight reduction (5–8 %) in rat body weight was observed 24 h after a cyclophosphamide loading dose (Data not shown). However, animals recovered weight before receiving the first cyclophosphamide maintenance dose. For the respiratory function, respiratory wheezing was graded into mild, faint, moderate; audible with normal respiratory rate, and severe; audible with rapid respiratory rate. Cyclophosphamide exerted no effect on rat respiratory function as demonstrated in the absence of wheeze for non-infected groups who received saline or LNPs.

3.4.3. Inoculum size and route of inoculation

Trials to induce IPA in neutropenic rats were performed to assess the most appropriate route of inoculation of fungal load achieving reproducible delivery of the inoculum to the lungs. These included intranasal (**Group I),** orotracheal (**Group II)** and intratracheal instillation (**Group III).** Although the intranasal inoculation closely resembles the route of natural infection in humans, it failed to induce any infection in the cultivated lungs of neutropenic rats. These results were in agreement with Revelli *et al.* who reported the unsuitability of the intranasal route in the induction of pulmonary melioidosis as the majority of the inoculated dose remained within the rat's nasal passages or was removed through the gastrointestinal tract (Revelli et al., 2012). Moreover, the intranasal route could develop the risk of disease dissemination and migration into the central nervous system.

Non-invasive (oral endotracheal, **group II)** or invasive (intratracheal, **group III**) inoculations offer alternative routes bypassing the rat nasal passages with the advantage of the introduction of a known load directly into the lungs. Non-invasive orotracheal inoculation presented less risk to the investigator and required less training and less time for the procedure. Although the infection was successfully induced by this method of inoculation, the results revealed wide variability in fungal burden upon mycological investigation of the dissected lungs. This can be attributed to the mucociliary clearance mechanism which can expel as many as 1.0×10^8 conidia per day (Desoubeaux and Cray, 2018). With invasive intratracheal installation, the fungal inoculum was controlled reproducibly and deposited in a sinopulmonary organ bypassing the conducting airways and their putative defenses with minimal surgery. Hence, intratracheal instillation via tracheotomy was selected as the method of infection.

The size of A. fumigatus inoculum for the experimental challenge represents an additional source of variability. A dose-dependent infection severity was reported relevant to the number of conidia in the inoculum (Dixon et al., 1989). In preliminary studies, intratracheal challenge via tracheotomy, **group III,** was achieved with a 5×10^7 conidia dose. This dose induced lethal aspergillosis within 48–72 h. Accordingly, lower doses; 5×10^6 and 5×10^5 inoculum sizes, **groups IV** and **V** respectively, were investigated. $1–4 \times 10^4$ CFU/lung were retrieved without death, demonstrating optimal dose: mortality ratios. In contrast, no or minimal growth, 100 CFU/lung, was observed upon inoculating with 5×10^4 spore suspension in **group VI**.

Owing to the relative reproducibility of the intratracheal instillation in inoculation and retrieval of fungal burden, we adopted it as the route of fungal instillation of 5×10^6 CFU/100 μL. We thereby administered daily doses **(D_2-D_9)** of DPPC/DMPG-VRZ-LNPs via oral endotracheal administration.

3.4.4. Survival and clinical manifestations

It remains controversial whenever it comes to assessing the invasive fungal burden in infected rodents. Ethical committees encourage adopting different methodologies and endpoints. However, mortality persists to be the most straightforward estimate for the assessment of fungal load progression (Desoubeaux and Cray, 2017). There was no spontaneous death in the two uninfected groups; saline-treated **(UN)** and VRZ treated **(UT)**, over 10 days period. All neutropenic uninfected animals survived throughout the experiments till $\mathbf{D_{10}}$. This confirms that despite the successful induction of neutropenia indicated by the blood picture, such immunocompromise was not lethal to the animals. On the other hand, mortality was up to 100 % 6 days post-infection in neutropenic infected rats receiving intrapulmonary saline, **IN group** as shown in Fig. 5**A**. Local treatment with **PL^2-S7** at 1 mg/kg daily dose for 8 days post-infection, $\mathbf{D_2}$ - $\mathbf{D_9}$, resulted in a remarkable reduction in the mortality rate; 40 % of the animals survived 6 days post infection, whereas ~ 33.3 % survived the experimental period. The survival curve of the treated group **(IT)** was significantly different ($P = 0.026$) from the non-treated group **(IN)** using the Log-rank (Mantel-Cox) test, suggestive of the effective role of DPPC/DMPG-VRZ-LNPs containment of the fatal pulmonary fungal infection.

Monitoring clinical signs of disease progression, it was noted that a 20–25 % reduction in body weight and/or development of severe respiratory wheezing were recognized as strong predicting signs for death within 24 h. Compared to the uninfected groups which demonstrated constant body weight with slight fluctuations, neutropenic infected groups demonstrated remarkable weight loss over the study period, Table 5**A**. The Infected/Non-Treated group **(IN)** lost up to ~ 22 % of their body weight by $\mathbf{D_5}$. Reduction in body weight ≥ 20 % of the baseline is a vital marker for severe infection (Desoubeaux and Chandenier, 2012). On the other hand, the Infected/Treated **(IT)** group showed a controlled pattern of weight loss up to $\mathbf{D_7}$ (-8.45 ± 2.31 %) then deteriorated to ~ 18 % by the end of study $\mathbf{D_{10}}$. This suggests that the DPPC/DMPG-VRZ-LNPs contained the fungal infection and prevented it from posing an extra risk factor for rats' health. These results are in good agreement with previously published studies reporting marked weight loss with the development of pulmonary diseases (Chandenier et al., 2009; Desoubeaux and Cray, 2018). However, the last maintenance dose of cyclophosphamide **(D_7)** might have contributed to weight loss (<20 % by $\mathbf{D_{10}}$).

The neutropenic uninfected/Non-Treated **(UN)** group showed a very faint breathing sound observed after $\mathbf{D_{10}}$ (Table 5**B**), indicating slight damage in lung tissues following continuous saline doses. Interestingly, this sound was not detectable in the Uninfected/Treated group **(UT)** treated by **PL^2-S7**. On the other hand**,** neutropenic infected groups showed mild respiratory wheezing starting from $\mathbf{D_2}$. However, in the case of saline-treated group (**IT**), the wheezing progressed rapidly into moderate followed by severe loud wheezing which was observed just a few hours before recording death. It must be noted that the severity of wheezing was previously correlated with the degree of fungal invasiveness (Chandenier et al., 2009). Accordingly, the respiratory distress can be ascribed to the fungal infection manifestations in immunocompromised rats rather than cyclophosphamide doses. For the **PL^2-S7** treated group, **IT**, the wheezing remained under control (mild) during the 10 days experimental period. This indicates the rapid efficacy of the local treatment succeeding in preventing the fatal risk of pulmonary *Aspergillus* infection.

3.4.5. Biochemical and histological analyses

Mortality persists to be the main clinical outcome of IPA, particularly in therapeutic assays. However, alternative endpoints may be evaluated to predict the fungal load (Desoubeaux and Cray, 2017). Galactomannan antigen **(GM)** determination and histopathological examination appear reliable and largely validated, in comparison with other surrogate biomarkers (Mercier et al., 2018; Stolz et al., 2018). GM is a fungal cell wall polysaccharide that *Aspergillus* species can release during growth or even

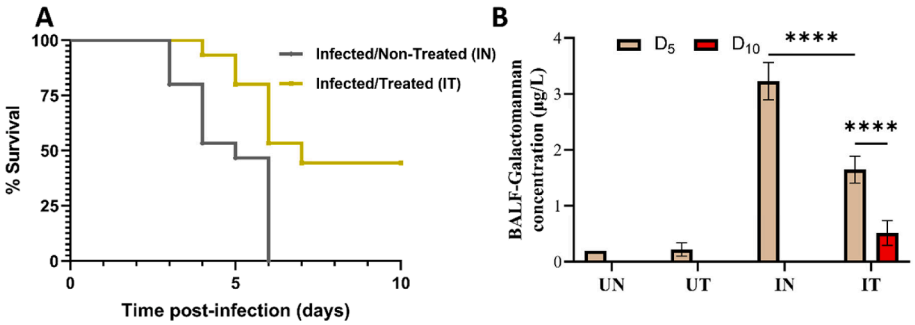

Fig. 5. A. Animal survival curve of neutropenic Sprague Dawley rats infected with 5×10^6 CFU/100 µL *A. fumigatus* and treated with intrapulmonary saline (Infected/Non-Treated Group: IN) or DPPC/DMPG-VRZ-LNPs (Infected/Treated Group: IT) (n = 15). Survival Curves were statistically significant following the Log-rank, Mantel-Cox test (p = 0.0044). B. Galactomannan concentration (µg/L) in broncho-alveolar lavage fluid (BALF) samples from immunocompromised rats, mean ± SD, n = 3. Two-way ANOVA followed by Tukey's multiple comparisons. Data were considered significant at $p < 0.05$.

Table 5
Clinical manifestations of IPA in a neutropenic rat model. (A) Variation in body weight relevant to the initial weight on D_0, (B) Development of respiratory wheezing sounds.

Animal Group	% Change in body weight* (A)								
	D_2	D_3	D_4	D_5	D_6	D_7	D_8	D_9	D_{10}
Uninfected/Non-Treated (UN)	+6.35±4.5				+4.75±3.2				-6.97±1.9
Uninfected/Treated (UT)	+5.72±0.48				-1.98±3.79				-7.8±2.91
Infected/Non-Treated (IN)	-7.97±1.81	-15.83±3.52	-20.08±2.11	-22.33±1.04					
Infected/Treated (IT)	-6.34±1.61	-12.18±1.5	-13.5±1.5	-13.45±1.26	-11.33±1.35	-8.45±2.31	-12.56±2.35	-16.83±1.83	-18.3±1.42

* Relative to body weight at D_0
(-) Weight loss, (+) Weight gain

Animal Group	Respiratory wheezing (B)								
	D_2	D_3	D_4	D_5	D_6	D_7	D_8	D_9	D_{10}
Uninfected/Non-Treated (UN)	Absent								+
Uninfected/Treated (UT)	Absent								
Infected/Non-Treated (IN)	+	++	++	+++					
Infected/Treated (IT)	+	+	+	+	+	+	+	+	+

(+) Mild, (++) Moderate, (+++) Severe

* Relative to body weight at D_0.
(-) Weight loss, (+) Weight gain
(+) Mild, (++) Moderate, (+++) Severe.

in the early stages of infection. It is considered as an important surrogate marker for the early diagnosis and monitoring of IPA, regardless of the involved species of *Aspergillus* (Taghizadeh-Armaki et al., 2017). However, the sensitivity of GM in the case of *A. flavus;* the second most common etiological agent of invasive aspergillosis, is much lower when compared to *A. fumigatus* (Rudramurthy et al., 2019). Becker *et al.* demonstrated that the quantitative GM detection in the rat model of IPA was superior to PCR in diagnosis as well as monitoring IPA in both blood and BALF samples (Becker et al., 2000). BALF-GM assay is more sensitive in detecting pulmonary aspergillosis than serum-GM assay (Musher et al., 2004; Zhang et al., 2015).

Under general anesthesia and at predetermined time intervals, bronchial lavage was performed to quantify GM. Fig. 5**B** shows that BALF-GM concentrations less than 0.5 µg/L, a cutoff value of positive infection as reported by Meersseman *et al.* (Meersseman et al., 2008), were observed on **D_5** in all control uninfected groups, **UN** and **UT**. Significantly higher BALF-GM concentrations (p-value < 0.0001) were observed in infected rats with saline treatment (**IN** group: 3.23 ± 0.145 µg/L, range: 2.9–3.56 µg/L) compared to values after DPPC/DMPG-VRZ-LNPs treatment (**IT** group: 1.65 ± 0.24 µg/L, range: 1.41–1.89 µg/L). Interestingly, 10 days post-infection, **D_{10}**, surviving rats in the DPPC/DMPG-VRZ-LNPs treated group showed more than a 3-fold reduction in BALF-GM concentration (p-value < 0.0001) compared to **D_5** results (0.515 ± 0.22 µg/L, range 0.32–0.72 µg/L) confirming their potential in hyphal growth inhibition, as GM is released predominantly from hyphae and in much lesser quantities from conidia (Becker et al., 2000; Meersseman et al., 2008). Thereby pulmonary administration of DPPC/DMPG-VRZ-LNPs contributes to the reduction of the fungal invasiveness

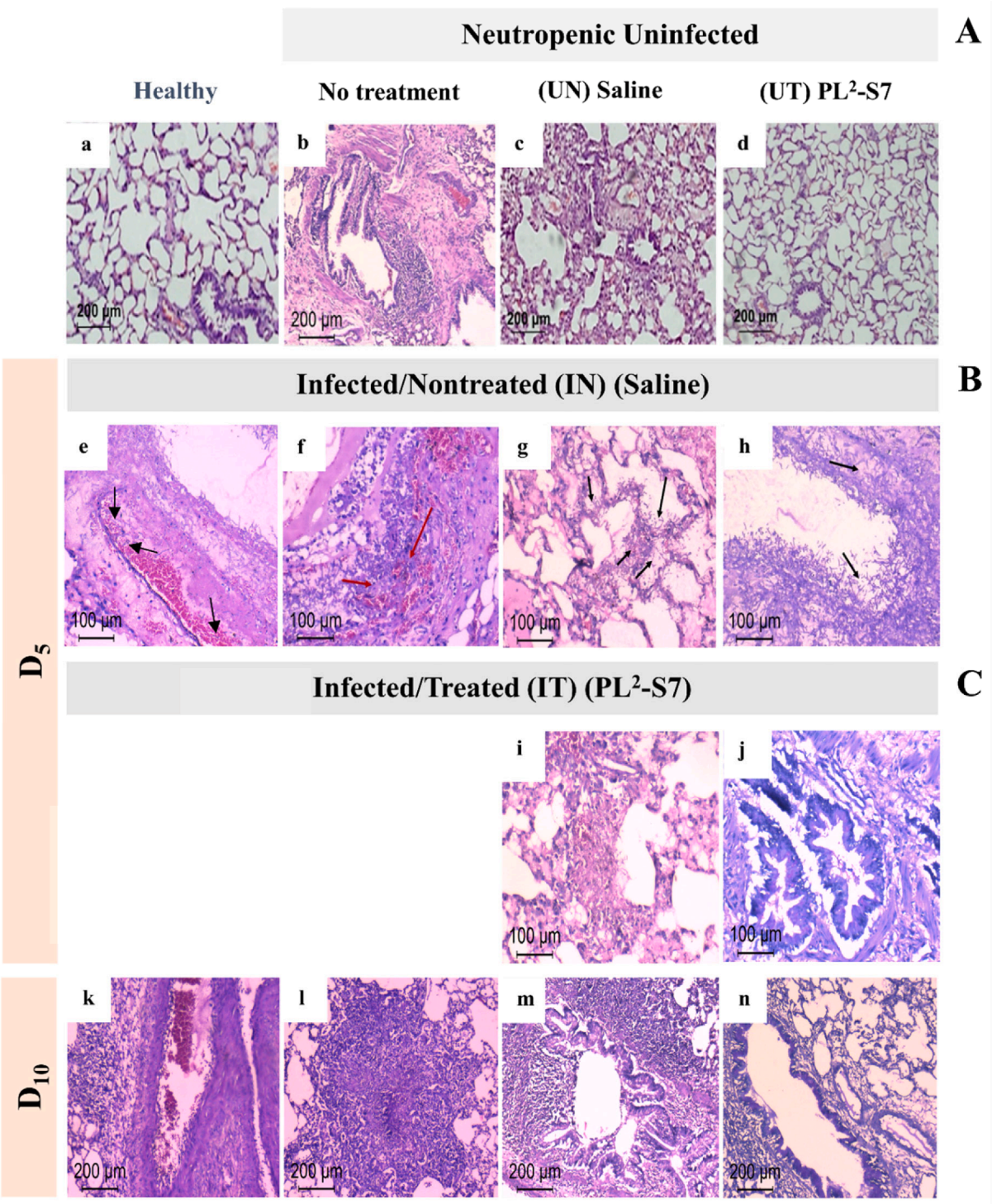

Fig. 6. Histopathological lung sections examination in neutropenic rat model. (A) Representative images of Hematoxylin and eosin, H&E staining of uninfected lung sections retrieved from (a) Healthy naive Sprague Dawley rats or (b-d) neutropenic uninfected rat groups (D_{10} post neutropenia): (b) no treatment, (c) daily intrapulmonary saline (Uninfected/Nontreated-UN) showing thick alveolar septum with inflammatory cells infiltrates, or (d) daily intrapulmonary PL^2-S7 equivalent to 1 mg VRZ/Kg body weight (Uninfected/Treated-UT) showing relatively thinner alveolar septum. (B-C) Neutropenic Sprague Dawley rats infected with 5×10^6 CFU/100 µL *A. Fumigatus* and treated daily with intrapulmonary (B) saline (IN) or (C) PL^2-S7 dispersion equivalent to 1 mg VRZ/Kg body weight (IT). (B) shows Hematoxylin and eosin H&E staining (e-g) and Periodic Acid-Schiff, PAS staining (h) D_5 post fungal infection, black arrows indicate fungi, and red arrows indicate tissue necrosis. (C) shows representative lung sections on D_5 (H&E: i, PAS: j) or D_{10} (H&E: k-m, PAS: n).

in the lungs of immunocompromised animals for management and prophylaxis against IPA.

Fig. 6**A$_{b-d}$** shows representative histopathological evaluation of H&E-stained lung sections of neutropenic uninfected rats receiving no treatment **(**Fig. 6**b),** saline (UN) **(Fig. c),** or **PL^2-S7** (UT) **(**Fig. 6**d)** compared to naïve lung sections from healthy non-immunocompromised rats **(**Fig. 6**a).** Segmental pneumonia was demonstrated as a thickening in the interaction septum with a mild

increase in inflammatory cell infiltrates in the **UN** group. This can explain the slight weight loss and the faint breathing sounds observed with the final doses of saline. **UT** lung section images revealed recovery of pneumonia in terms of the restoration of the thickness of interaction septa, minimum cellular infiltrates, and residual congestion**.** This improvement may be attributed to the composition of the administered lipid nanoparticles, mainly DPPC. Indeed, the effectiveness of exogenous surfactant therapy had previously been demonstrated in children with respiratory failure due to severe pneumonia (Mikawa et al., 1993). Birkun *et al.* observed an enhanced anti-inflammatory effect with intratracheal administration of an amikacin-lung surfactant mixture; composed of purified phospholipids, isolated from porcine lung homogenates to rats with *Pseudomonas* pneumonia compared to amikacin without lung surfactant (Birkun, 2014; BirkunAlexei et al., 2014). Furthermore, Anzueto *et al.,* demonstrated improvement in lung function and oxygenation upon aerosolization of DPPC (Anzueto et al., 1997). Accordingly, DPPC/DMPG surface-modified VRZ-LNPs can exert a dual function in controlling the infection and improving the deteriorated respiratory function associated with the infection in immunocompromised rats.

Fig. 6**B$_{e-h}$** illustrates lung sections **(on D_5)** from infected rat groups receiving no antifungal treatment, **IN** group. They show dense fungal load with disseminated mycelial filaments. Fungal hyphae proliferated inside dilatated bronchioles, alveoli**,** interalveolar spaces, and even in blood vessels, indicating massive tissue and angio-invasiveness. Moreover, severe tissue necrosis was detected with mild inflammation (Fig. 6**f**). For better fungal visualization, PAS stain, a special fungal stain, was utilized. *Aspergillus* infection was demonstrated as long-branched septate hyphae with almost uniform diameter, Fig. 6**h.**

In contrast, the DPPC/DMPG-VRZ-LNPs treated group **(IT)**; Fig. 6**C$_{i-n}$**, exhibited a minimal load of fungal hyphae in alveoli, interstitial spaces, and bronchioles with no signs of severe tissue invasiveness on both **D_5** and **D_{10}** post-infection. Clear blood vessels shown in Fig. 6**k** indicated controlled angio-invasiveness. Infection adopted a localized granular form with mild focal tissue necrosis as shown in Fig. 6**i**. It is worth noting that similar degrees of inflammation and leukocytic infiltration were observed for all infected groups. Accordingly, the improvement detected in the treated groups can be directly attributed to PL^2-S7 effectiveness at low inhalation dose (1 mg/kg) rather than the immune state of the test animals.

4. Conclusions

In the present work, we optimized DPPC/DMPG surface-modified compritol lipid nanoparticles to serve as bioactive targeting carriers for the local pulmonary administration of voriconazole. We introduced a pulmonary-active delivery platform for VRZ as a biomimetic approach with an eye on the natural lung surfactant pool. This was executed to increase particles' pulmonary tolerability and to minimize the risk of macrophage uptake. The inclusion of DPPC with or without moderate proportions of DMPG (<10 % w/w surface coat) resulted in enhanced VRZ entrapment and shelf storage stability. Formulation-wise, surface modification using DPPC/DMPG phospholipid blend improved the spray drying/aerosolization parameters. This was further reflected in the *in vitro* VRZ lung deposition using a cascade impactor to reflect terminal bronchi and alveolar ducts targeting. Moreover, DPPC/DMPG-VRZ-LNPs released VRZ in a sustained release manner over 24 h favorable for pulmonary local administration than the VRZ-LNPs which showed a fast burst release. DPPC/DMPG modified particles showed optimal retention in the lungs after 6 h, unlike free drug which was rapidly absorbed into the systemic circulation. *In vivo* preclinical studies affirmed the invasive role of pulmonary aspergillosis in immunocompromised candidates. However, pulmonary administration of DPPC/DMPG-VRZ-LNPs demonstrated optimal containment of fungal infection and enhanced survival rate. The developed system bestows localized targeted delivery at a reduced tolerable inhalation dose (1 mg/Kg), minimized systemic toxicity, with limited drug-drug interactions of VRZ as a treatment and/or prophylactic therapy for pulmonary aspergillosis in the immunocompromised population.

Funding information

This work was supported by the Academic Thesis Research Fund (ATRF), Faculty of Pharmacy, Alexandria University (ATRF-319011) .

CRediT authorship contribution statement

Heba A. Fayyaz: Data curation, Formal analysis, Funding acquisition, Investigation, Methodology, Validation, Visualization, Writing – original draft, Project administration, Resources. **Magda A. EL-Massik:** Conceptualization, Supervision, Writing – review & editing, Validation, Methodology. **Mohammed Bahey-El-Din:** Conceptualization, Formal analysis, Investigation, Methodology, Visualization. **Amany Abdel-Bary:** Conceptualization, Formal analysis, Investigation, Validation. **Ossama Y. Abdallah:** Project administration, Resources, Supervision, Validation, Methodology. **Hoda M. Eltaher:** Conceptualization, Data curation, Formal analysis, Funding acquisition, Investigation, Methodology, Project administration, Resources, Supervision, Validation, Visualization, Writing – review & editing.

Declaration of competing interest

The authors declare that they have no known competing financial interests or personal relationships that could have appeared to influence the work reported in this paper.

Data availability

Data will be made available on request.

Appendix A. Supplementary data

Supplementary data to this article can be found online at https://doi.org/10.1016/j.ijpharm.2023.123663.

References

Agudelo, C.W., Samaha, G., Garcia-Arcos, I., 2020. Alveolar lipids in pulmonary disease. A review. Lipids Health Dis. 19, 122.

Anzueto, A., Jubran, A., Ohar, J., Piquette, C., Rennard, S., Colice, G., Pattishall, E., Barrett, J., Engle, M., Perret, K.A., Rubin, B., 1997. Effects of aerosolized surfactant in patients with stable chronic bronchitis: A prospective randomized controlled trial. JAMA 278, 1426–1431.

Arastehfar, A., Carvalho, A., Houbraken, J., Lombardi, L., Garcia-Rubio, R., Jenks, J.D., Rivero-Menendez, O., Aljohani, R., Jacobsen, I.D., Berman, J., Osherov, N., Hedayati, M.T., Ilkit, M., Armstrong-James, D., Gabaldón, T., Meletiadis, J., Kostrzewa, M., Pan, W., Lass-Flörl, C., Perlin, D.S., Hoenigl, M., 2021. Aspergillus fumigatus and aspergillosis: From basics to clinics. Stud. Mycol. 100, 100115.

Becker, M.J., de Marie, S., Willemse, D., Verbrugh, H.A., Bakker-Woudenberg, I.A.J.M., 2000. Quantitative galactomannan detection is superior to PCR in diagnosing and monitoring invasive pulmonary aspergillosis in an experimental rat model. J. Clin. Microbiol. 38, 1434.

Bellmann, R., Smuszkiewicz, P., 2017. Pharmacokinetics of antifungal drugs: practical implications for optimized treatment of patients. Infection 45, 737–779.

Birkun, A., 2014. Exogenous pulmonary surfactant as a vehicle for antimicrobials: Assessment of surfactant-antibacterial interactions in vitro. Scientifica 2014, 930318.

BirkunAlexei, A., KubyshkinAnatoly, V., NovikovNikolai, Y., KrivorutchenkoYuri, L., FedosovMichael, I., PostnikovaOlga, N., SnitserAnatoly, A., 2014. Joint intratracheal surfactant-antibacterial therapy in experimental pseudomonas-induced pneumonia. J. Aerosol Med. Pulm. Drug Deliv. 28, 299–307.

Borghardt, J.M., Kloft, C., Sharma, A., 2018. Inhaled therapy in respiratory disease: The complex interplay of pulmonary kinetic processes. Can Respir J 2018, 2732017.

Budin, S., Salmanton-Garcia, J., Koehler, P., Stemler, J., Cornely, O.A., Mellinghoff, S.C., 2021. Validation of the EQUAL aspergillosis Score by analysing guideline-adherent management of invasive pulmonary aspergillosis. J Antimicrob Chemother 76, 1070–1077.

Chabi, M.L., Goracci, A., Roche, N., Paugam, A., Lupo, A., Revel, M.P., 2015. Pulmonary aspergillosis. Diagnostic and Interventional Imaging 96, 435–442.

Chandenier, J., Bernard, S., Montharu, J., Bailly, E., Fetissof, F., Monte, M., Desoubeaux, G., Diot, P., Richard-Lenoble, D., 2009. The utility of a nebulised intratracheal rat model of invasive pulmonary aspergillosis. Mycoses 52, 239–245.

Chauvin, D., Hust, M., Schütte, M., Chesnay, A., Parent, C., Moreira, G.M.S.G., Arroyo, J., Sanz, A.B., Pugnière, M., Martineau, P., Chandenier, J., Heuzé-Vourc'h, N., Desoubeaux, G., 2019. Targeting aspergillus fumigatus Crf transglycosylases with neutralizing antibody is relevant but not sufficient to erase fungal burden in a neutropenic rat model. Frontiers in Microbiology 10.

Chen, X., Xiao, Y., Li, H., Huang, Z., Gao, J., Zhang, X., Li, Y., Van Timothee, B.M., Feng, X., 2022. Therapeutic drug monitoring and CYP2C19 genotyping guide the application of voriconazole in children. Transl Pediatr 11, 1311–1322.

Chen, Z., Zhong, M., Luo, Y., Deng, L., Hu, Z., Song, Y., 2019. Determination of rheology and surface tension of airway surface liquid: A review of clinical relevance and measurement techniques. Respir. Res. 20, 274.

Cuvelier, B., Eloy, P., Loira-Pastoriza, C., Ucakar, B., Sanogo, A.A., Dupont-Gillain, C., Vanbever, R., 2015. Minimal amounts of dipalmitoylphosphatidylcholine improve aerosol performance of spray-dried temocillin powders for inhalation. Int J Pharm 495, 981–990.

Deng, Z., Kalin, G.T., Shi, D., Kalinichenko, V.V., 2021. Nanoparticle delivery systems with cell-specific targeting for pulmonary diseases. Am J Respir Cell Mol Biol 64, 292–307.

Desoubeaux, G., Chandenier, J., 2012. A nebulized intra-tracheal rat model of invasive pulmonary aspergillosis. Methods in molecular biology (Clifton. N.J.) 845, 511–518.

Desoubeaux, G., Cray, C., 2017. Rodent models of invasive aspergillosis due to aspergillus fumigatus: Still a long path toward standardization. Front. Microbiol. 8, 841.

Desoubeaux, G., Cray, C., 2018. Animal models of aspergillosis. Comp Med 68, 109–123.

Dixon, D.M., Polak, A., Walsh, T.J., 1989. Fungus dose-dependent primary pulmonary aspergillosis in immunosuppressed mice. Infect. Immun. 57, 1452–1456.

Duan, J., Vogt, F.G., Li, X., Hayes Jr., D., Mansour, H.M., 2013. Design, characterization, and aerosolization of organic solution advanced spray-dried moxifloxacin and ofloxacin dipalmitoylphosphatidylcholine (DPPC) microparticulate/nanoparticulate powders for pulmonary inhalation aerosol delivery. Int J Nanomedicine 8, 3489–3505.

El-Melegy, M.G., Eltaher, H.M., Gaballah, A., El-Kamel, A.H., 2021. Enhanced oral permeability of trans-resveratrol using nanocochleates for boosting anticancer efficacy; in-vitro and ex-vivo appraisal. Eur J Pharm Biopharm 168, 166–183.

El-Sherbiny, I., Guzman-Villanueva, D., Herrera-Ruiz, D., Smyth, H., 2011. Overcoming lung clearance mechanisms for controlled release drug delivery. Controlled Pulmonary Drug Delivery 101–126.

Firacative, C., 2020. Invasive fungal disease in humans: are we aware of the real impact? Mem Inst Oswaldo Cruz 115, e200430.

Fisher, A., 2015. Lung Lipid Composition and Surfactant Biology. Second Edition, Comparative Biology of the Normal Lung, pp. 423–466.

Freeman Weiss, Z., Leon, A., Koo, S., 2021. The evolving landscape of fungal diagnostics, current and emerging microbiological approaches. J Fungi 7, 127.

Ghali, M.G.Z., 2018. Microsurgical technique for tracheostomy in the rat. MethodsX 5, 61–67.

Ghasemiyeh, P., Mohammadi-Samani, S., 2018. Solid lipid nanoparticles and nanostructured lipid carriers as novel drug delivery systems: Applications, advantages and disadvantages. Res Pharm Sci 13, 288–303.

Guagliardo, R., Pérez-Gil, J., De Smedt, S., Raemdonck, K., 2018. Pulmonary surfactant and drug delivery: Focusing on the role of surfactant proteins. J. Control. Release 291, 116–126.

Guillon, A., Secher, T., Dailey, L.A., Vecellio, L., de Monte, M., Si-Tahar, M., Diot, P., Page, C.P., Heuze-Vourc'h, N., 2018. Insights on animal models to investigate inhalation therapy: Relevance for biotherapeutics. Int J Pharm 536, 116–126.

Habicht, J.M., Preiss, M., Passweg, J., Dalquen, P., Matt, P., Adler, H., Frei, R., Zerkowski, H.R., 2002. Invasive pulmonary aspergillosis: Effects of early resection in a neutropenic rat model. Eur. J. Cardiothorac. Surg. 22, 728–732.

He, S., Gui, J., Xiong, K., Chen, M., Gao, H., Fu, Y., 2022. A roadmap to pulmonary delivery strategies for the treatment of infectious lung diseases. J Nanobiotechnology 20, 101.

Hidalgo, A., Garcia-Mouton, C., Autilio, C., carravilla, p., Orellana, G., Islam, M., Bhattacharya, J., Bhattacharya, S., Cruz, A., Perez-Gil, J., 2020. Pulmonary surfactant and drug delivery: Vehiculization, release and targeting of surfactant/tacrolimus formulations. J. Control. Release 329.

Ishak, R.A.H., Osman, R., 2015. Lecithin/TPGS-based spray-dried self-microemulsifying drug delivery systems: In vitro pulmonary deposition and cytotoxicity. Int J Pharmaceut 485, 249–260.

Jiang, L., Lee, H.W., Loo, S.C.J., 2020. Therapeutic lipid-coated hybrid nanoparticles against bacterial infections. RSC Adv 10, 8497–8517.

Joshi, N., Shirsath, N., Singh, A., Joshi, K.S., Banerjee, R., 2014. Endogenous lung surfactant inspired pH responsive nanovesicle aerosols: Pulmonary compatible and site-specific drug delivery in lung metastases. Sci. Rep. 4, 7085.

Jović, Z., Janković, S.M., Ružić Zečević, D., Milovanović, D., Stefanović, S., Folić, M., Milovanović, J., Kostić, M., 2019. Clinical pharmacokinetics of second-generation triazoles for the treatment of invasive aspergillosis and candidiasis. Eur. J. Drug Metab. Pharmacokinet. 44, 139–157.

Kaur, R., Dennison, S.R., Burrow, A.J., Rudramurthy, S.M., Swami, R., Gorki, V., Katare, O.P., Kaushik, A., Singh, B., Singh, K.K., 2021. Nebulised surface-active hybrid nanoparticles of voriconazole for pulmonary Aspergillosis demonstrate clathrin-mediated cellular uptake, improved antifungal efficacy and lung retention. J Nanobiotechnology 19, 19.

Khan, A.A., Abdulbaqi, I.M., Abou Assi, R., Murugaiyah, V., Darwis, Y., 2018. Lyophilized hybrid nanostructured lipid carriers to enhance the cellular uptake of verapamil: Statistical optimization and in vitro evaluation. Nanoscale Res Lett 13, 323.

Khetre, A.B., Sinha, P.K., Damle, M.C., Mehendre, R., 2009. Development and validation of stability indicating RP-HPLC method for voriconazole. Indian J Pharm Sci 71, 509–514.

Kirkpatrick, W.R., Wiederhold, N.P., Najvar, L.K., Patterson, T.F., 2013. Animal models in mycology: what have we learned over the past 30 years. Current Fungal Infection Reports 7, 68–78.

Kousha, M., Tadi, R., Soubani, A.O., 2011. Pulmonary aspergillosis: A clinical review. Eur. Respir. Rev. 20, 156.

Krishnamachari, Y., Madan, P., Lin, S.S., 2007. Development of pH- and time-dependent oral microparticles to optimize budesonide delivery to ileum and colon. Int J Pharmaceut 338, 238–247.

Kumar, B., Ahmad, F., Mittal, G., Jain, G., Malhotra, G., Khar, R., Bhatnagar, A., 2008. Nano-salbutamol dry powder inhalation: A new approach for treating broncho-constrictive conditions. European Journal of Pharmaceutics and Biopharmaceutics : Official Journal of Arbeitsgemeinschaft Für Pharmazeutische Verfahrenstechnik E.v 71, 282–291.

Kwok, P.C., Chan, H.K., 2014. Nanotechnology versus other techniques in improving drug dissolution. Curr Pharm Des 20, 474–482.

Lat, A., Thompson 3rd, G.R., 2011. Update on the optimal use of voriconazole for invasive fungal infections. Infect Drug Resist 4, 43–53.

Latgé, J.P., Chamilos, G., 2019. Aspergillus fumigatus and aspergillosis in 2019. Clin Microbiol Rev 33.

Li, Z., Qiao, W., Wang, C., Wang, H., Ma, M., Han, X., Tang, J., 2020. DPPC-coated lipid nanoparticles as an inhalable carrier for accumulation of resveratrol in the pulmonary vasculature, a new strategy for pulmonary arterial hypertension treatment. Drug Deliv 27, 736–744.

Lo Giudice, P., Campo, S., Verdoliva, A., Rivieccio, V., Borsini, F., De Santis, R., Salvatori, G., 2010. Efficacy of PTX3 in a rat model of invasive aspergillosis. Antimicrob Agents Chemother 54, 4513–4515.

Ma, X., Zhang, S., Xing, H., Li, H., Chen, J., Li, H., Jiao, M., Shi, Q., Xu, A., Xing, L., Cao, W., 2022. Invasive pulmonary aspergillosis diagnosis via peripheral blood metagenomic next-generation sequencing. Front Med (lausanne) 9, 751617.

Mangal, S., Gao, W., Li, T., Zhou, Q.T., 2017. Pulmonary delivery of nanoparticle chemotherapy for the treatment of lung cancers: Challenges and opportunities. Acta Pharmacol Sin 38, 782–797.

McClements, D.J., Jafari, S.M., 2018. Improving emulsion formation, stability and performance using mixed emulsifiers: A review. Adv Colloid Interface Sci 251, 55–79.

Meersseman, W., Lagrou, K., Maertens, J., Wilmer, A., Hermans, G., Vanderschueren, S., Spriet, I., Verbeken, E., Van Wijngaerden, E., 2008. Galactomannan in bronchoalveolar lavage fluid. Am. J. Respir. Crit. Care Med. 177, 27–34.

Mercier, T., Guldentops, E., Lagrou, K., Maertens, J., 2018. Galactomannan, a surrogate marker for outcome in invasive aspergillosis: Finally coming of age. Front. Microbiol. 9.

Merlos, R., Amighi, K., Wauthoz, N., 2014. Recent developments in inhaled triazoles against invasive pulmonary aspergillosis. Current Fungal Infection Reports 8, 331–342.

Michael, C., Bierbach, U., Frenzel, K., Lange, T., Basara, N., Niederwieser, D., Mauz-Korholz, C., Preiss, R., 2010. Voriconazole pharmacokinetics and safety in immunocompromised children compared to adult patients. Antimicrob Agents Chemother 54, 3225–3232.

Mikawa, K., Maekawa, N., Nishina, K., Takao, Y., Yaku, H., Obara, H., 1993. Selective intrabronchial instillation of surfactant in a patient with pneumonia: A preliminary report. Eur. Respir. J. 6, 1563.

Mishra, B., Singh, J., 2020. Novel drug delivery systems and significance in respiratory diseases. Targeting Chronic Inflammatory Lung Diseases Using Advanced Drug Delivery Systems 57–95.

Mitchell, J.P., Stein, S.W., Doub, W., Goodey, A.P., Christopher, J.D., Patel, R.B., Tougas, T.P., Lyapustina, S., 2019. Determination of passive dry powder inhaler aerodynamic particle size distribution by multi-stage cascade impactor: International pharmaceutical aerosol consortium on regulation & science (IPAC-RS) recommendations to support both product quality control and clinical programs. AAPS PharmSciTech 20.

Mousavi, B., Hedayati, M.T., Hedayati, N., Ilkit, M., Syedmousavi, S., 2016. Aspergillus species in indoor environments and their possible occupational and public health hazards. Curr Med Mycol 2, 36–42.

Muralidharan, P., Malapit, M., Mallory, E., Hayes, D., Mansour, H.M., 2015. Inhalable nanoparticulate powders for respiratory delivery. Nanomedicine: Nanotechnology Biology and Medicine 11, 1189–1199.

Musher, B., Fredricks, D., Leisenring, W., Balajee, S.A., Smith, C., Marr, K.A., 2004. Aspergillus galactomannan enzyme immunoassay and quantitative PCR for diagnosis of invasive aspergillosis with bronchoalveolar lavage fluid. J. Clin. Microbiol. 42, 5517–5522.

Nakmode, D., Bhavana, V., Thakor, P., Madan, J., Singh, P.K., Singh, S.B., Rosenholm, J. M., Bansal, K.K., Mehra, N.K., 2022. Fundamental aspects of lipid-based excipients in lipid-based product development. Pharmaceutics 14.

Nandini, C., Madhunapantula, SubbaRao V., Bovilla, Venugopal R., Mohammad Ali, K., Mruthunjaya, Manjula N., Santhepete, K. Jayashree, 2021. Platelet enhancement by Carica papaya L. leaf fractions in cyclophosphamide induced thrombocytopenic rats is due to elevated expression of CD110 receptor on megakaryocytes. J. Ethnopharmacol. 275, 114074 https://doi.org/10.1016/j.jep.2021.114074. ISSN 0378- 8741.

Newman, S.P., 2017. Drug delivery to the lungs: Challenges and opportunities. Ther Deliv 8, 647–661.

Orssaud, C., Guillemain, R., Lillo Le Louet, A., 2021. Toxic optic neuropathy due to voriconazole: Possible potentiation by reduction of CYP2C19 activity. Eur Rev Med Pharmacol Sci 25, 7823–7828.
Osibe, D., Lei, S., Wang, B., Jin, C., Fang, W., 2020. Cell wall polysaccharides from pathogenic fungi for diagnosis of fungal infectious disease. Mycoses 63.
Osman, R., Al Jamal, K.T., Kan, P.L., Awad, G., Mortada, N., El-Shamy, A.E., Alpar, O., 2013. Inhalable DNase I microparticles engineered with biologically active excipients. Pulm Pharmacol Ther 26, 700–709.
Pichot, R., Watson, R.L., Norton, I.T., 2013. Phospholipids at the interface: current trends and challenges. Int J Mol Sci 14, 11767–11794.
Pramanik, S., Mohanto, S., Manne, R., Rajendran, R.R., Deepak, A., Edapully, S.J., Patil, T., Katari, O., 2021. Nanoparticle-based drug delivery system: The magic bullet for the treatment of chronic pulmonary diseases. Mol Pharm 18, 3671–3718.
Revelli, D., Boylan, J., Gherardini, F., 2012. A non-invasive intratracheal inoculation method for the study of pulmonary melioidosis. Frontiers in Cellular and Infection Microbiology 2.
Ribeiro, R.S.A., Ferreira, I.M.E.S.R., Figueiredo Jr, I., Verícimo, M.A., 2015. Access to the tracheal pulmonary pathway in small rodents. Jornal Brasileiro De Patologia e Medicina Laboratorial 51, 183–188.
Rudramurthy, S.M., Paul, R.A., Chakrabarti, A., Mouton, J.W., Meis, J.F., 2019. Invasive aspergillosis by aspergillus flavus: Epidemiology, diagnosis antifungal resistance, and management. J Fungi (basel) 5.
Sanguinetti, M., Posteraro, B., 2018. Susceptibility testing of fungi to antifungal drugs. J Fungi 4.
Sharma, N., Madan, P., Lin, S.S., 2016. Effect of process and formulation variables on the preparation of parenteral paclitaxel-loaded biodegradable polymeric nanoparticles: A co-surfactant study. Asian J Pharm Sci 11, 404–416.
Sou, T., Kukavica-Ibrulj, I., Soukarieh, F., Halliday, N., Levesque, R.C., Williams, P., Stocks, M., Cámara, M., Friberg, L.E., Bergström, C.A.S., 2019. Model-based drug development in pulmonary delivery: pharmacokinetic analysis of novel drug candidates for treatment of pseudomonas aeruginosa lung infection. J. Pharm. Sci. 108, 630–640.
Stolz, D.J., Sands, E.M., Amarsaikhan, N., Tsoggerel, A., Templeton, S.P., 2018. Histological quantification to determine lung fungal burden in experimental aspergillosis. J vis Exp 57155.
Taghizadeh-Armaki, M., Hedayati, M.T., Moqarabzadeh, V., Ansari, S., Mahdavi Omran, S., Zarrinfar, H., Saber, S., Verweij, P.E., Denning, D.W., Seyedmousavi, S., 2017. Effect of involved Aspergillus species on galactomannan in bronchoalveolar lavage of patients with invasive aspergillosis. J Med Microbiol 66, 898–904.
Turk, C.T.S., Oz, U.C., Serim, T.M., Hascicek, C., 2014. Formulation and optimization of nonionic surfactants emulsified nimesulide-loaded PLGA-based nanoparticles by design of experiments. AAPS PharmSciTech 15, 161–176.
Veldhuizen, R., Nag, K., Orgeig, S., Possmayer, F., 1998. The role of lipids in pulmonary surfactant. Biochim. Biophys. Acta (BBA) - Mol. Basis Dis. 1408, 90–108.
Verweij, P.E., Rijnders, B.J.A., Brüggemann, R.J.M., Azoulay, E., Bassetti, M., Blot, S., Calandra, T., Clancy, C.J., Cornely, O.A., Chiller, T., Depuydt, P., Giacobbe, D.R., Janssen, N.A.F., Kullberg, B.J., Lagrou, K., Lass-Flörl, C., Lewis, R.E., Liu, P.W., Lortholary, O., Maertens, J., Martin-Loeches, I., Nguyen, M.H., Patterson, T.F., Rogers, T.R., Schouten, J.A., Spriet, I., Vanderbeke, L., Wauters, J., van de Veerdonk, F.L., 2020. Review of influenza-associated pulmonary aspergillosis in ICU patients and proposal for a case definition: An expert opinion. Intensive Care Med 46, 1524–1535.
Vijayanand, P., Jyothi, V., Aditya, N., Mounika, A., 2018. Development and characterization of solid lipid nanoparticles containing herbal extract: In Vivo antidepressant activity. J Drug Deliv, 2908626. https://doi.org/10.1155/2018/2908626. PMID: 29973993; PMCID: PMC6008679.
Walsh, T.J., Karlsson, M.O., Driscoll, T., Arguedas, A.G., Adamson, P., Saez-Llorens, X., Vora, A.J., Arrieta, A.C., Blumer, J., Lutsar, I., Milligan, P., Wood, N., 2004. Pharmacokinetics and safety of intravenous voriconazole in children after single- or multiple-dose administration. Antimicrob Agents Chemother 48, 2166–2172.
Wauthoz, N., Amighi, K., 2014. Phospholipids in pulmonary drug delivery. Eur. J. Lipid Sci. Technol. 1114–1128.
Zakaria, A., Osman, M., Dabboussi, F., Rafei, R., Mallat, H., Papon, N., Bouchara, J.-P., Hamze, M., 2020. Recent trends in the epidemiology, diagnosis, treatment, and mechanisms of resistance in clinical Aspergillus species: A general review with a special focus on the middle eastern and north african region. J. Infect. Public Health 13, 1–10.
Zhang, S., Wang, S., Wan, Z., Li, R., Yu, J., 2015. The diagnosis of invasive and noninvasive pulmonary aspergillosis by serum and bronchoalveolar lavage fluid galactomannan assay. Biomed Res Int 2015, 943691.